AEDC-TDR-64-134

1 of 3

INFLUENCE OF PERTINENT PARAMETERS ON EJECTOR-DIFFUSER PERFORMANCE WITH AND WITHOUT EJECTED MASS

77 pp $3.00 hc
$0.75 mf

By

James W. Hale

Rocket Test Facility

ARO, Inc.

TECHNICAL DOCUMENTARY REPORT NO. AEDC-TDR-64-134

July 1964

Program Element 62405184

(Prepared under Contract No. AF 40(600)-1000 by ARO, Inc., contract operator of AEDC, Arnold Air Force Station, Tenn.)

ARNOLD ENGINEERING DEVELOPMENT CENTER

AIR FORCE SYSTEMS COMMAND

UNITED STATES AIR FORCE

NOTICES

Qualified requesters may obtain copies of this report from DDC, Cameron Station, Alexandria, Va. Orders will be expedited if placed through the librarian or other staff member designated to request and receive documents from DDC.

When Government drawings, specifications or other data are used for any purpose other than in connection with a definitely related Government procurement operation, the United States Government thereby incurs no responsibility nor any obligation whatsoever; and the fact that the Government may have formulated, furnished, or in any way supplied the said drawings, specifications, or other data, is not to be regarded by implication or otherwise as in any manner licensing the holder or any other person or corporation, or conveying any rights or permission to manufacture, use, or sell any patented invention that may in any way be related thereto.

AEDC-TDR-64-134

INFLUENCE OF PERTINENT PARAMETERS ON EJECTOR-DIFFUSER PERFORMANCE WITH AND WITHOUT EJECTED MASS

By

James W. Hale

Rocket Test Facility

ARO, Inc.

a subsidiary of Sverdrup and Parcel, Inc.

July 1964

ARO Project Nos. RM1306, RK0245, RM1146

ABSTRACT

Data from various diffuser model studies were analyzed to determine the influence of pertinent parameters on ejector-diffuser performance with and without ejected mass from the test cell. The parameters varied were conical nozzle area ratio (3.15 to 18.00), diffuser shape (straight or with various types of bends), mass ejected from the test cell (from 0.11 to 1.31 percent of rocket flow) for different nozzle configurations (single-, two-, and four-nozzle cluster) and diffuser sizes (4.026- to 10.02-in. diam), and ratio of diffuser-to-nozzle exit area on start and breakdown diffuser pressure ratio with respect to second-throat contraction ratio.

The cell-to-driving fluid total pressure ratios increased with decreasing nozzle area ratio (for a given diffuser-to-nozzle throat area ratio). The effective length-to-diameter ratio, on which the driving pressure ratio at start and breakdown depends, varied with the severity of the bend in the diffuser. Diffusers with long gradual turns performed like long, straight diffusers, and those with short sudden turns performed like short, straight diffusers. Mass ejection from the test cell resulted in a small variation in cell-to-driving total pressure ratio as compared with the variation of cell-to-driving total pressure ratio without mass ejection for corresponding variations in diffuser-to-nozzle throat area ratio with various nozzle configurations. The limiting second-throat contraction ratio (A_{st}/A_d) increased with increasing diffuser-to-nozzle exit area ratio for the nozzle configurations tested. When the diffuser-to-nozzle exit area ratio was equal to or greater than 6, the spacing of the second throat from the nozzle exit became very critical. The start and breakdown pressure ratio can be affected by only a small change in the spacing of the second throat from the nozzle exit. The position of the second throat for such configurations with a large duct-to-nozzle exit area ratio (greater than 6) determines the amount of improvement in start and breakdown pressure ratio.

PUBLICATION REVIEW

This report has been reviewed and publication is approved.

Eules L. Hively
Eules L. Hively
Acting Chief, Propulsion Division
DCS/Research

D. R. Eastman, Jr.
Donald R. Eastman, Jr.
DCS/Research

CONTENTS

TABLES

ILLUSTRATIONS

NOMENCLATURE

A_d	Cross-sectional area of diffuser, $in.^2$
A_{ne}	Cross-sectional area of nozzle exit, $in.^2$
A_{st}	Cross-sectional area of second throat duct, $in.^2$
A^*	Cross-sectional area of nozzle throat, $in.^2$
D	Diameter of diffuser duct, in.
d^*	Diameter of nozzle throat, in.
d_{ne}	Diameter of nozzle exit, in.
d	Diameter of diffuser second-throat duct, in.
L	Length of diffuser duct at diameter, D, in. (unless otherwise noted)
ℓ	Length of diffuser second-throat duct at diameter, d, in.
M_b	Free-jet boundary Mach number
M_d	Diffuser duct Mach number
M_{ne}	Simulated nozzle exit Mach number
P_c	Simulated rocket test cell pressure, psia
P_{c1}	Jet pump number 1 cell or secondary pressure, psia
P_{c2}	Jet pump number 2 cell or secondary pressure, psia
P_t	Simulated rocket chamber total pressure, psia
P_{t1}	Jet pump number 1 driving or primary pressure, psia
P_{t2}	Jet pump number 2 driving or primary pressure, psia
P_{ex}	Diffuser duct exit pressure, psia
T_t	Simulated rocket driving fluid total temperature, °F
T_{t1}	Jet pump number 1 driving fluid total temperature, °F
T_{t2}	Jet pump number 2 driving fluid total temperature, °F
W_a	Simulated rocket mass flow rate, lb_m/sec
W_b	Jet pumps total ejected or secondary mass flow rate, lb_m/sec
W_p	Jet pumps total driving fluid or primary mass flow rate, lb_m/sec
X	Distance from the nozzle exit to the beginning of the second throat, in.

Z	Distance from nozzle exit to diffuser inlet (Minus sign indicates that the diffuser inlet is upstream of the nozzle exit, and plus sign indicates that the diffuser inlet is downstream of the nozzle exit.), in.
α	Flow direction angle of free-jet boundary at the nozzle lip with respect to the centerline of flow, deg
β	Flow direction angle of free-jet boundary on diffuser impingement region with respect to the centerline of the flow, deg
γ	Ratio of specific heats
δ	Total angle through which the jet boundary turns from the nozzle exit to the diffuser wall ($\alpha - \beta$), deg
θ_n	Nozzle divergent half angle, deg
ν	Prandtl-Meyer stream expansion angle, deg
σ	Rate of spread of the mixing region ($\sigma = 12 + 2.758\ M_b$)

SUBSCRIPTS

act	Actual
st	Second throat
ns	Normal shock
isen	Isentropic
j	Condition at nozzle exit before expansion (inside the jet and calculated from isentropic flow relations)
x	Upstream of normal shock
y	Downstream of normal shock

SUPERSCRIPT

'	Ejected mass from the simulated rocket test cell

1.0 INTRODUCTION

The engineer is faced with the problem of seeking economical techniques to extend ground facility testing capabilities to meet the present-day rocket test requirements. Such a technique for facility improvement is the development of the ejector-diffuser system which allows rockets to be tested at much higher simulated altitude conditions than are possible with existing ground facility capabilities alone.

Although many problems have been resolved in determining the ejector-diffuser design parameters, the technique has not yet reached the point of perfection. The influence of pertinent varied parameters on ejector-diffuser performance imposed by the rocket test requirements is still being documented.

An investigation was conducted through model studies to determine the influence of certain pertinent parameters on ejector-diffuser performance both with and without ejected mass from the test cell. The parameters studied are:

1. Variation of nozzle area ratio, A_{ne}/A^*,
2. Diffuser shape or geometry (straight or with various types of bends),
3. Mass ejection from the test cell for different nozzle configurations and diffuser sizes, and
4. Ratio of diffuser-to-nozzle exit area, A_d/A_{ne}, on start and breakdown pressure ratio, P_{ex}/P_t, with respect to second-throat contraction ratio, A_{st}/A_d.

Seven nozzle configurations (single-, two-, and four-nozzle clusters) in combination with eight diffuser configurations were used in this investigation. Correlation between experimental data and one-dimensional relationships for diffuser-to-nozzle throat area ratio, cell-to-nozzle total pressure ratio, and ratio of specific heats is shown.

This study was conducted in the Propulsion Research Area (R-2D) of the Rocket Test Facility (RTF), Arnold Engineering Development Center (AEDC), Air Force Systems Command (AFSC), from August 21, 1962, to August 22, 1963.

Manuscript received June 1964.

2.0 APPARATUS

The eight basic diffuser test configurations used in this investigation were driven by a simulated rocket nozzle configuration selected from a group of seven which consisted of either a single-, two-, or four-nozzle cluster.

2.1 SIMULATED ROCKET TEST CELL

The Propulsion Research Area (R-2D) consists of a duct 12 in. in diameter and 21 in. long, to which two parallel air-driven auxiliary jet pumps are perpendicularly attached 180 deg apart as shown in Fig. 1. The jet pumps discharge through the facility exhaust ducting downstream of the hand-operated isolation valve. Two 4-in. gate valves separate the test cell from the jet pumps.

Each jet pump consists of an axisymmetric 9-deg half-angle conical nozzle attached to a plenum chamber section fabricated from a 1-1/2-in. schedule double, extra heavy pipe approximately 13 in. long and installed inside the 4-in. standard schedule 40 ducts as shown in Fig. 1a. The nozzles for both pumps are identical, with throat diameters of 0.437 in. The nozzle exit-to-throat area ratio of each jet pump is 25.12. Complete details of the jet pump nozzles are presented in Fig. 4 of Ref. 1.

2.2 SIMULATED ROCKET NOZZLE PLENUM SECTION

The simulated rocket nozzles were installed on a 4-in. schedule 160 pipe welded to a 6-in. flange. The different nozzles were connected to the plenum section as shown in Fig. 2. The nozzle configuration was installed in a sealed plenum or test cell section to which the diffuser was attached. A typical test configuration is shown in Fig. 1.

2.3 SIMULATED ROCKET NOZZLE CONFIGURATIONS

The axisymmetric conical nozzles used in the seven nozzle configurations are similar to those used in Ref. 1. The nozzles are shown in detail in Fig. 3, and a description of the nozzles and the seven nozzle configurations is given in Table 1.

2.4 DUCT AND NOZZLE DESIGNATION

The eight basic diffuser configurations are shown in Fig. 4. A description of the type of diffusers, the configuration numbers, and

dimensional details are shown in Table 2. Included in the Summary of Test Data (Tables 3 and 4) are the duct and nozzle configuration code designations of the nozzle and diffuser combinations. The duct and nozzle configuration code designation combines the nozzle configuration code (Fig. 2 and Table 1) and the diffuser configuration code (Fig. 4 and Table 2). A typical duct and nozzle configuration designation as listed in Table 3 is 1-A (diffuser configuration 1 from Fig. 4 and Table 2, and nozzle configuration A from Fig. 2 and Table 1). The S preceding the diffuser configuration code as in Fig. 4b and Tables 2 and 4 designates the second-throat diffuser for the diffuser configuration 3.

2.5 DIFFUSER INSTALLATION

The 24-in. space shown in Fig. 1a exists between the downstream face of the test cell and the upstream face of the exhaust ducting for installation of the various diffuser configurations. This space was utilized for installation of the straight cylindrical and second-throat diffuser configurations (configurations 1, 2, 3, S3, 4, and 5). A modified installation arrangement (Figs. 1b through d) was made for the diffuser configurations with bends (configurations 6, 7, and 8).

2.5.1 Constant Area Cylindrical and Second-Throat Diffuser Configurations

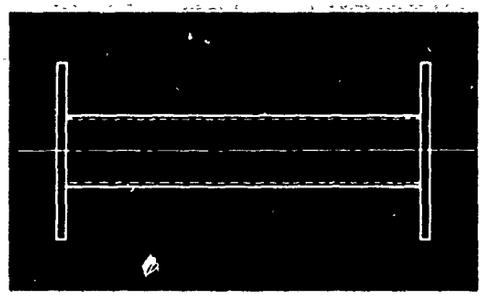

Configurations 1 and 3

Five sizes of constant area cylindrical diffusers were investigated. The dimensional details of two of the five are presented in Fig. 4a as configurations 1 and 3 with corresponding diameters of 4.026 and

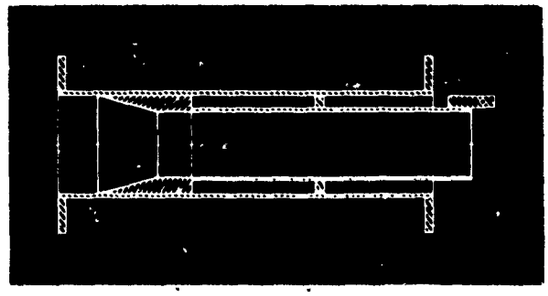

Configuration S3

6.141 in. A second-throat insert was installed in diffuser configuration 3 and designated as configuration S3. Three second-throat diffuser inserts (diameters: 4.026, 4.625, 4.943 in. as shown in Fig. 4b and Table 2) were investigated with the diffuser configuration 3. The position of the second throat from the nozzle exit was made variable by sliding the second-throat insert inside the 6.141-in. duct (configuration 3 diffuser) by a linkage mechanism located in the first spool piece of the exhaust ducting shown in Fig. 1b.

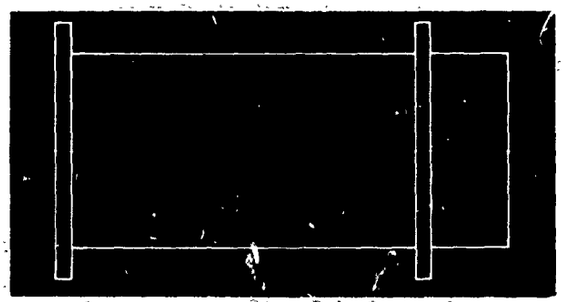

Configurations 2, 4, and 5

Diffuser configurations 2, 4, and 5 (Fig. 4c) have 4.680, 8.092, and 10.02-in. diameters, respectively. The flanges were placed 24 in. apart to correspond to the space between the test cell and exhaust ducting shown in Fig. 1a.

2.5.2 Constant-Area Cylindrical Diffusers with Bends

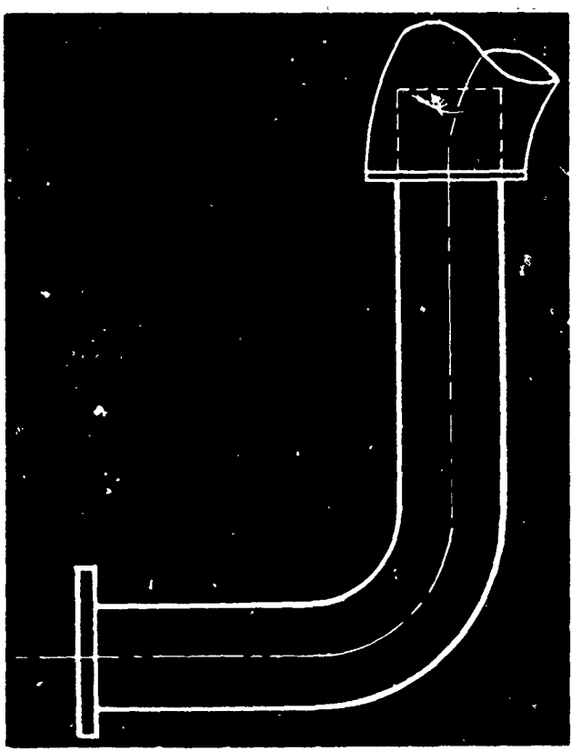

Configuration 6

A 5.763-in.-diam, constant-area cylindrical diffuser with a 90-deg long radius elbow (Fig. 4d) was designated as configuration 6. A 15.5-in. straight diffuser section was upstream of the bend, and a 27.75-in. section was downstream of the bend.

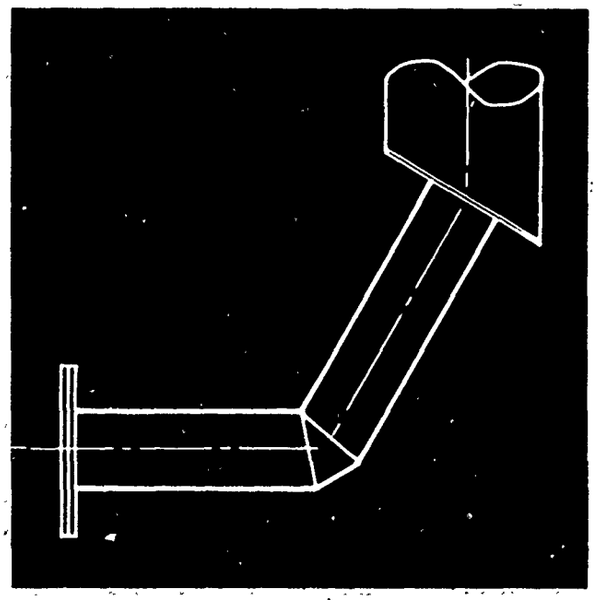

Configuration 7

Configuration 7 (Fig. 4e) consisted of a 4.647-in.-diam, constant-area cylindrical diffuser with a 60-deg total-angle miter bend. A length of 15.75 in. of straight duct was upstream of the bend and 16.88 in. downstream of the bend.

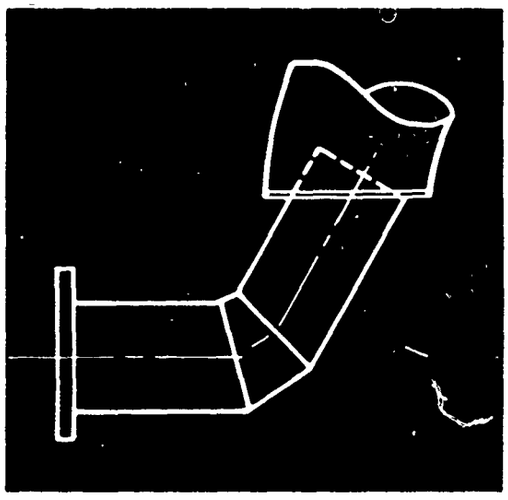

Configuration 8

Configuration 8 (Fig. 4f) consisted of a 5.763-in.-diam, constant-area cylindrical diffuser with a 60-deg total-angle miter bend. The

length of the straight diffuser section upstream of the bend was 11.43 in. and downstream of the bend was 11.53 in.

2.6 SIMULATED ROCKET NOZZLE AND JET PUMP DRIVING FLUID

Air from the VKF 4000-psi storage tank or 200-psig saturated steam from the AEDC central plant provided the driving medium for the simulated rocket nozzles with a plenum total pressure as high as 192 psia with steam and 403 psia with air. The same air from the VKF 4000-psi storage tank provided the driving medium for the jet pumps at an optimum driving pressure of 70 psia, which discharged to the RTF exhaust machines. The ejector-diffusers exhausted to the RTF exhaust machines, which maintained a pressure as low as 0.12 psia. The 20-in., hand-operated gate valve (Fig. 1) was used to vary the exhaust pressure at the exit of the ejector-diffuser.

2.7 INSTRUMENTATION

The parameters of primary interest were cell pressures for the two jet pumps and the ejector-diffusers, P_{c1}, P_{c2}, and P_c; diffuser exit pressure, P_{ex}; jet pump and simulated rocket nozzle plenum total pressures, P_{t1}, P_{t2}, and P_t; and plenum total temperature for the jet pumps and simulated rocket nozzles, T_{t1}, T_{t2}, and T_t.

All pressures were read on diaphragm-activated dial gages. These gages were periodically calibrated, and the readings were well within the calibration range. The temperatures were measured with copper-constantan thermocouples and read on compensating millivolt meters. All parameters were recorded manually after a steady-state condition was reached.

2.8 JET PUMP CALIBRATION

As reported in Ref. 1, a calibration of the jet pumps was accomplished by installing a flange of five venturis on the inlet to the jet pump cell valve, which connects the jet pump to the test cell (Fig. 1). The five venturis were used to measure the atmospheric inbleed or secondary airflow into the jet pump cell region. The secondary airflow was varied by inbleeding through one or more of the five venturis. Rubber plugs were used to isolate the venturis for varying the secondary airflow.

The jet pump cell or secondary pressure was measured for the various atmospheric inbleed airflows for a range of jet pump driving

pressures with both air and steam as the jet pump driving medium. The jet pump calibration was used to determine the ejected mass flow from the test cell for the configuration being tested.

3.0 TEST PROCEDURE

At the beginning of each test, a vacuum check was made to detect any possible leaks into the system before data were taken.

The test objective was to measure the performance of each test configuration as an ejector-diffuser by finding the minimum cell-to-nozzle total pressure ratio, P_c/P_t, and the corresponding starting and operating pressure ratios, P_{ex}/P_t, in order to determine the effect on performance of the various parameters. Such parameters were (1) variation in nozzle area ratio, A_{ne}/A^*, (2) diffuser shape (straight or with various types of bends), (3) mass ejection from the test cell for different nozzle configurations and diffuser sizes, and (4) effects of variation of the ratio of duct-to-nozzle exit, A_d/A_{ne}, on start and breakdown pressure ratio with respect to second-throat contraction ratio, A_{st}/A_d. A typical ejector performance curve defining the starting and operating pressure ratios is presented in Fig. 3 of Ref. 2.

The data were obtained by setting the desired nozzle plenum total pressure with the exhaust pressure set low enough to ensure ejector starting (minimum P_c/P_t as obtained for diffusers with no second throat) and then increasing the exhaust pressure until an increase in cell pressure was noted (ejector unstarted). This point determined the operating pressure ratio. The exhaust pressure was then decreased until the ejector became started. This point determined the starting pressure ratio.

3.1 IMPROVED PERFORMANCE BY JET PUMPS

Various configurations were tested to determine the decrease in minimum pressure ratio, P_c/P_t, by ejecting mass from the test cell with the jet pumps. While the diffuser was started and operating at its minimum pressure ratio, P_c/P_t, and while the jet pumps were operated at no secondary flow, one (or both) of the 4-in., hand-operated valves between the ejector-diffuser test cell and the jet pump cell region was opened. The maximum decrease in P_c/P_t occurred when both jet pumps were pumping at maximum efficiency with valves opened to the test cell. The starting and operating driving pressure ratio, P_{ex}/P_t, was determined with the jet pumps ejecting mass from the test cell for comparison with the no-ejected mass condition.

3.2 EFFECT OF SECOND-THROAT POSITIONING

The variable axial position second-throat diffuser configurations (S3a, S3b, and S3c) were tested with nozzle configurations A, B3, B4, C, and D at various positions to determine the optimum location from the nozzle exit to the beginning of the second throat for the ejector-diffuser to operate at the minimum pressure ratio, P_c/P_t. In the vicinity of the position for minimum P_c/P_t, the start and breakdown pressure ratio, P_{ex}/P_t, was determined.

4.0 RESULTS AND DISCUSSION

The primary purpose of this investigation was to determine the effect of a change in various parameters on the ejector-diffuser performance. Such parameter changes include (1) nozzle area ratio, (2) diffuser shape and size (straight or with various types of bends), (3) mass ejection from test cell for different nozzle configurations and diffuser sizes, and (4) the effect of diffuser-to-nozzle exit area ratio on start and breakdown pressure ratio for various second-throat contraction ratios.

A summary of the data from the configurations tested and the experimental results compared with one-dimensional isentropic values from Ref. 3 is presented in Tables 3 and 4 and in Figs. 5 through 13.

4.1 NOZZLE AREA RATIO INFLUENCE ON EJECTOR-DIFFUSER PERFORMANCE

Ejector-diffuser tests were conducted with nozzle configuration B1 ($A_{ne}/A^* = 5.00$) from Table 1 driving different size, constant-area diffusers (Tables 2 and 3). The nozzles were identical except for area ratio, A_{ne}/A^*, which resulted in a nozzle exit Mach number, M_{ne}, difference as shown in Table 3 since the one-dimensional isentropic Mach number relationship is a direct function of nozzle area ratio and the ratio of specific heats or $M_{ne} = f(A_{ne}/A^*, \gamma)$.

Presented in Fig. 5a is the performance of two different nozzle configurations driving the same size diffuser (4.026-in.-diam) configuration. A difference in cell-to-nozzle total pressure ratio, P_c/P_t, is evident. The P_c/P_t for configuration 1-B2 ($A_{ne}/A^* = 5.00$) is higher than the P_c/P_t for configuration 1-B1 ($A_{ne}/A^* = 18.00$) by a factor of 1.52.

The driving pressure ratio, P_{ex}/P_t, for configuration 1-B2 is 8-percent lower than that for configuration 1-B1. The L/D's for the

two configurations are essentially equal (Table 3). This lower P_{ex}/P_t for configuration 1-B2 means that the diffuser will break down at a lower diffuser exit pressure than will configuration 1-B1 for the same given nozzle driving pressure. Presented in Fig. 5b is the performance of B1 and B2 nozzle configurations driving a larger diffuser (8.092-in.-diam) configuration 4. There is essentially no difference in the P_{ex}/P_t for configurations 4-B1 and 4-B2. The P_{ex}/P_t performance for the B1 and B2 nozzle configuration driven ejector-diffusers in relation to the one-dimensional normal shock total pressure ratio, P_{ty}/P_{tx}, is presented in Fig. 11a. This P_{ex}/P_t performance line is almost parallel to the $\gamma = 1.40$ one-dimensional normal shock total pressure ratio line and is approximately 69.30 percent of P_{ty}/P_{tx}. The variation of $P_{ex}/P_t/P_{ty}/P_{tx}$ with L/D as compared with the results presented in Ref. 1 is shown in Fig. 12a. The trend of the data is identical to that in Ref. 1.

The P_c/P_t ejector-diffuser performance for the two nozzle configurations (B1, $A_{ne}/A^* = 18.00$, and B2, $A_{ne}/A^* = 5.00$) in different size ducts is presented in Fig. 10a in relation to their isentropic values. Since the diffuser-to-nozzle throat area ratios, A_d/A^*, are the same for either one of the two nozzle configurations driving the same diffuser configuration, the corresponding isentropic values are the same as shown in Fig. 10a.

The P_c/P_t for configuration 4-B2 is higher than that for configuration 4-B1 by a factor of 1.85. The difference in P_c/P_t for the large diffuser (configuration 4) is larger than that for the small diffuser (configuration 1).

Nozzle configuration B1 ($A_{ne}/A^* = 18.00$) was tested with five diffuser sizes. Their performance almost parallels the isentropic curve $\gamma = 1.40$ except for the two larger A_d/A^* configurations (4-B1 and 5-B1). From Table 3, the ratio $(P_c/P_t)_{act}/(P_c/P_t)_{isen}$ for the different configurations is as follows:

Configuration	$(P_c/P_t)_{act}/(P_c/P_t)_{isen}$
1-B1	1.198
2-B1	1.270
4-B1	1.749
5-B1	2.742
6-B1	1.320

The straight line trend of the points for configurations 1-B1, 2-B1, and 6-B1 is the same as that presented in Refs. 1 and 4. The increased deviation of the cell-to-nozzle driving pressure ratio from the isentropic value as shown in Fig. 10a for configurations 4-B1 and 5-B1 is probably

a result of the driving fluid condensation effect as discussed in Ref. 5 and the increased rate of spread of the mixing region as discussed in Refs. 6 and 7.

Nozzle configuration B2 ($A_{ne}/A^* = 5.00$) was tested with three diffuser configurations (1, 3, and 4). The P_c/P_t performance for these configurations is presented in Fig. 10a. A higher P_c/P_t by an average factor of 1.68 was obtained for these configurations (1-B2, 3-B2, and 4-B2) than was obtained for the diffuser configurations with nozzle configurations B1 (1-B1, 2-B1, 4-B1, 5-B1, and 6-B1). The deviation of P_c/P_t from the one-dimensional isentropic value given in Table 3 is as follows:

Configuration	$(P_c/P_t)_{act}/(P_c/P_t)_{isen}$
1-B2	1.785
3-B2	2.673
4-B2	3.242

A P_c/P_t linear increase deviation from the one-dimensional isentropic value resulted for both the B1 and B2 nozzle configurations. (The performance lines diverge for increasing A_d/A^*.) This result was probably an effect of the increased length of the free-jet mixing zone for the increase in A_d/A^*. The difference in P_c/P_t performance for the two nozzles (B1 and B2) as shown in Fig. 10a is a probable result of the change in the rate of spread of the mixing region referred to as σ since the nozzle exit Mach numbers are different. References 6 and 7 show that the value of σ is dependent on the free-jet boundary Mach number, M_b, such as $\sigma = 12 + 2.758\ M_b$ where $M_b = f(P_c/P_t, \gamma)$ as shown in Ref. 7.

From the jet boundaries calculated by the method in Ref. 8 for both nozzle configurations B1 and B2 driving diffuser configurations 1 and 4, the lengths along the jet boundaries were determined. No essential difference existed in the length of the free-jet boundaries for these nozzle configurations driving diffuser configuration 1. The difference in the length of the jet boundaries for the nozzle configurations driving diffuser configuration 4 is approximately 1 in. A definite increase in the impingement angle, β, of the jet boundary on the diffuser wall is evident for the decrease in A_{ne}/A^* (18.00 to 5.00). The angle, α, of the tangent to the jet boundary at the nozzle is increased by changing the nozzle A_{ne}/A^* from 18.00 to 5.00 even when P_c/P_t remains unchanged. This fact is shown by the following equations:

$$\alpha = \nu - \nu_j + \theta_n$$

$$\nu = f(P_c/P_t, \gamma)$$

$$\nu_j = f(A_{ne}/A^*, \gamma)$$

Since the nozzle half-angle, θ_n, is not changed by cutting the nozzle off from an $A_{ne}/A^* = 18.00$ to 5.00 and since P_c/P_t is assumed not to change, ν_j is the only influencing parameter to cause α to increase; however, P_c/P_t did change slightly resulting in a slightly smaller increase in α than if P_c/P_t had remained constant. The angle, α, is larger for the small A_{ne}/A^* nozzle than for the large A_{ne}/A^* nozzle (see sketch below). From the jet boundaries shown in the sketch for these configurations, the jet boundaries of the smaller nozzle ($A_{ne}/A^* = 5.00$) configuration turned through a larger angle and impinged on the duct at a larger angle. The larger impingement angle, β, allows more rejected mass from the mixing zone to be turned back into the test cell. This results in a mass-rejected, mass-scavenged equilibrium at a higher test cell pressure level.

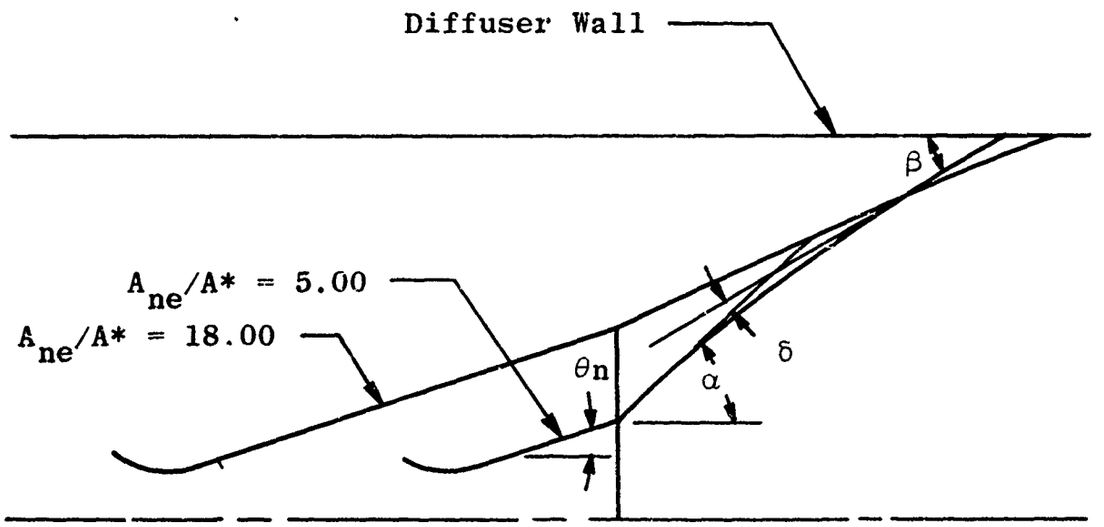

The same P_c/P_t and P_{ex}/P_t performance effect was experienced with nozzle configurations B3 and B4. The nozzles were identical, except the nozzle in configuration B4 (referred to as the scarf nozzle) had the exit cut at an angle other than perpendicular with the nozzle centerline, whereas the nozzle in configuration B3 (referred to as the straight exit nozzle) had an exit plane perpendicular to the nozzle centerline as shown in Figs. 2b and 3b. The scarf nozzle minimum and maximum exit diameters are 1.218 and 1.563 in., which correspond to nozzle area ratios of 2.38 and 3.914 (average $A_{ne}/A^* = 3.147$). The A_{ne}/A^* for the straight exit nozzle was 3.914. Since the nozzle exit Mach number is a function of A_{ne}/A^* and γ, there is a difference in the M_{ne} for the scarf ($M_{ne} = 2.69$) and straight exit ($M_{ne} = 2.92$) nozzles as shown in Table 3.

Both the straight exit nozzle configuration B3 and the scarf nozzle configuration B4 (Table 1) were used with the diffuser configurations 2, 3, 6, 7, and 8 (Table 2). The P_c/P_t and P_{ex}/P_t performance of the

individual ejector-diffuser configurations is presented in Fig. 7. Figures 7a and b present the performance of the straight diffuser configurations 2 and 3. The P_c/P_t for configurations 2-B4 and 3-B4 (scarf nozzle configurations) is higher than the P_c/P_t for configurations 2-B3 and 3-B3 (straight exit nozzle configurations) by a factor of 1.21 and 1.23, respectively. The breakdown pressure ratio, P_{ex}/P_t, for configurations 2-B4 and 3-B4 is lower than the P_{ex}/P_t for configurations 2-B3 and 3-B3 by a factor of 0.98 and 0.94, respectively. This decrease in ejector-diffuser performance is similar to the effect caused by reducing the A_{ne}/A^* from 18.00 to 5.00. Figures 7c, d, and e present the performance variation for diffuser configurations with bends (6, 7, and 8), driven by nozzle configurations B3 and B4. The P_c/P_t and P_{ex}/P_t performance difference for a particular diffuser with bends (6, 7, or 8) driven by either nozzle configuration B3 or B4 shows the same trend as did the straight diffuser configurations. The following table gives the loss in P_c/P_t and P_{ex}/P_t performance for the diffuser configurations with bends as a result of the effective nozzle area ratio change (from nozzle configuration B3 to B4).

Ejector-Diffuser Configuration	P_c/P_t Increase Factor	P_{ex}/P_t Decrease Factor
6-B3 to 6-B4	1.14	0.94
7-B3 to 7-B4	1.11	0.93
8-B3 to 8-B4	1.19	0.89

The P_c/P_t performance deviation from the one-dimensional isentropic value for the five diffuser configurations driven by nozzle configurations B3 and B4 is presented in Fig. 10b. The P_c/P_t performance lines for the two nozzle configurations B3 and B4 in the various diffusers are essentially parallel. The B4 nozzle configuration driven diffuser P_c/P_t performance is higher than that for the B3 nozzle configuration by an average factor of approximately 1.17. This average increase factor is lower than the approximate average value of 1.68 obtained for the B1 and B2 nozzle configuration driven diffusers shown in Fig. 10a. This difference in average increase factor for nozzle configurations B1 to B2 (1.68) and B3 to B4 (1.17) is a result of the difference in the average nozzle exit Mach number, M_{ne}, (B1 to B2, M_{ne} = 4.59 to 3.18 and B3 to B4, M_{ne} = 2.92 to 2.69) which affects the impingement angle, β. Nozzle configurations B1 and B2, which had the greatest change in M_{ne}, had the greatest average P_c/P_t increase factor.

The change in P_{ex}/P_t ratios is approximately equal for the straight diffuser configurations (2 and 3) and diffuser configurations with bends (6, 7, and 8) as a result of nozzle area ratio change (straight exit nozzle configuration B3 to scarf nozzle configuration B4) shown in Figs. 7a through e. This change in P_{ex}/P_t as a result of the nozzle area ratio

change (B3 to B4) is approximately equal to the change in P_{ex}/P_t obtained for configurations 1-B1 and 1-B2.

The start and breakdown pressure ratio, P_{ex}/P_t, performance for the B3 and B4 nozzle configuration driven ejector-diffusers in relation to the one-dimensional normal shock total pressure ratio, P_{ty}/P_{tx}, is presented in Fig. 11b. The data are more dispersed than those presented in Fig. 11a for nozzle configurations B1 and B2. This P_{ex}/P_t scatter will be shown and discussed in section 4.2 as an L/D effect. An average line through these points parallels the $\gamma = 1.40$ one-dimensional P_{ty}/P_{tx} line and is approximately 69.25 percent of P_{ty}/P_{tx}. This value is practically equal to the value obtained for the B1 and B2 nozzle configurations as shown in Fig. 11a (69.30 percent of P_{ty}/P_{tx}).

4.2 INFLUENCE OF DIFFUSER SHAPE AND SIZE ON EJECTOR-DIFFUSER PERFORMANCE

Both straight cylindrical diffusers and cylindrical diffusers with bends were investigated. Single-nozzle, two-nozzle, and four-nozzle configurations were used for driving the various diffuser configurations.

4.2.1 Effect of Diffuser Bends on Performance

The bend in the diffusers, such as configuration 7, apparently does not affect P_c/P_t performance, but P_{ex}/P_t is affected. This result is presented in Fig. 8 for configurations 2-B3 and 7-B3, which have very close to identical diameters ($A_d/A^* = 35.09$ for 2-B3 and 34.60 for 7-B3). The average total temperature of the driving fluid for 7-B3 was approximately 23°F lower than for 2-B3. This lower temperature driving fluid for configuration 7-B3 could possibly result in an increase in P_c/P_t over that for a higher driving fluid temperature as a result of fluid condensation effect (Ref. 5). The difference in A_d/A^* and the driving fluid temperature is considered responsible for the P_c/P_t difference shown for 2-B3 and 7-B3 in Fig. 8.

The effect of the bend on the P_{ex}/P_t performance as shown in Fig. 8 is the result of an effective change in the diffuser L/D. Even though diffuser configuration 7 (diffuser with bend, Fig. 4f) is longer than diffuser configuration 2 (straight diffuser, Fig. 4a), the effective length is shorter. The effective length of the diffuser with a bend is defined as the equivalent straight length required for a straight diffuser to give the same breakdown pressure ratio, P_{ex}/P_t, performance as that obtained for the diffuser with a bend. The effective length is approximately that length from the nozzle exit to the beginning of the bend. From Table 3, the L/D and $P_{ex}/P_t \,/\, P_{ty}/P_{tx}$ for these ejector-diffuser configurations is as follows:

Ejector-Diffuser Configuration	$\frac{P_{ex}/P_t}{P_{ty}/P_{tx}}$	L/D
2-B3	0.7309	5.33
7-B3	0.6503	3.27

This effective L/D change accounts for the difference in P_{ex}/P_t shown in Fig. 8 for the two configurations (2-B3 and 7-B3). A comparison of this variation of $P_{ex}/P_t \,/\, P_{ty}/P_{tx}$ with L/D in relation to the results in Ref. 1 is shown in Fig. 12b. Good agreement is evident.

Also shown in Fig. 12b is the $P_{ex}/P_t \,/\, P_{ty}/P_{tx}$ relationship with effective L/D for the diffuser configurations (2, 3, 6, 7, and 8) driven by both the B3 and B4 nozzle configurations. The trend parallels that in Ref. 1. This same spacing effect of a bend downstream of the nozzle exit on P_{ex}/P_t is presented in Ref. 9. The severity of the bend also affects the P_{ex}/P_t performance. This is shown in Table 3 and Fig. 12b for configurations 6-B3 and 8-B3, which are the same diameter diffusers but with different type bends (see Figs. 4d and f). From Fig. 12b, configuration 6 appears to have the higher breakdown performance, $P_{ex}/P_t/P_{ty}/P_{tx}$. This indicates that a diffuser with a long gradual bend performs more like a straight diffuser with the total centerline length as the effective length for calculating L/D. The effect of the radius of turn on the L/D is reported in Refs. 9 and 10. The severe shock patterns in the abrupt turns result in high pressure peaks in the elbow region. A diffuser with a long gradual turn as reported in Ref. 10 has a much milder shock pattern, resulting in a lower pressure in the elbow.

4.2.2 Two-Nozzle-Driven Diffuser Performance

In addition to the data in Ref. 1, more data were obtained for various size diffusers (configurations 3, 4, 5, and 6). Presented in Fig. 10c is the P_c/P_t performance for the different size diffusers both from this investigation and that reported in Ref. 1 in relation to the $\gamma = 1.40$ one-dimensional isentropic curve. A line through the experimental points diverges from the isentropic line for increasing A_d/A^*. This is a result observed in Refs. 1 and 4 and discussed in section 4.1 for the B1, B2, B3, and B4 nozzle configurations and shown in Figs. 10a and b. Isentropic P_c/P_t performance was obtained for the small A_d/A^* configuration.

The relationship of the breakdown pressure ratio, P_{ex}/P_t, for the different ejector-diffusers using the two-nozzle configuration A (Fig. 2a) is presented in Fig. 11c. The Ref. 1 data are closer to the $\gamma = 1.40$ one-dimensional normal shock total pressure ratio, P_{ty}/P_{tx}, line than the data obtained in this investigation. The ratio of $P_{ex}/P_t \,/\, P_{ty}/P_{tx}$ for the

two sets of data is shown in Table 3. The averages from Fig. 11c for the two sets of data are approximately 81 percent of P_{ty}/P_{tx} for Ref. 1 data and approximately 62 percent of P_{ty}/P_{tx} for the present data. This difference in P_{ex}/P_t can better be explained by considering the L/D effect for the configuration as shown in Ref. 1. Figure 12c presents this L/D relationship with $P_{ex}/P_t \,/\, P_{ty}/P_{tx}$ compared with the two-nozzle ejector-diffuser data taken from Fig. 10 of Ref. 1. These new data follow the same trend established in Ref. 1.

4.2.3 Four-Nozzle-Driven Diffuser Performance

Four-nozzle configuration C (Fig. 2c and Table 1) was used to drive a series of different diffusers (configurations 1 through 6). The P_c/P_t performance for this set of configurations follows a linear relationship similar to the single- and two-nozzle configurations previously discussed. The relation of the four-nozzle P_c/P_t performance to isentropic for the small A_d/A^* of 16.72 was similar to that obtained for the two-nozzle configuration A. The deviation of P_c/P_t for the four-nozzle configurations from the one-dimensional isentropic curve (Fig. 10c) for increasing A_d/A^* was greater than the corresponding deviation of P_c/P_t for the two-nozzle cluster (Fig. 10d). Since the two types of nozzle configurations (two- and four-nozzle cluster) differ essentially in $\Sigma(A_{ne}/A^*)$ as shown in Table 1, then the difference in P_c/P_t for the two- and four-nozzle configurations appears to be similar to the effect obtained for the single-nozzle configurations (B1 and B2 — B3 and B4) as discussed in section 4.1. A comparison of the performance for the different nozzle configurations from Fig. 10 shows that the larger the nozzle A_{ne}/A^* for essentially the same nozzle half-angle the lower the P_c/P_t will be regardless of whether one-, two-, or four-nozzle clusters are used for any particular A_d/A^*. This comparison is shown in Fig. 10d for the different nozzle configurations (A_{ne}/A^* = 18.00, 12.01, 5.00, and 4.12).

The P_{ex}/P_t for the diffuser configurations (1 through 6) using four-nozzle configuration C (Table 1) is presented in Fig. 11d. The data lie on a line which parallels the γ = 1.40 one-dimensional normal shock total pressure ratio line, approximately 67.5 percent of P_{ty}/P_{tx}. Since there was a variation in the L/D for the different ejector-diffuser configurations, these data can be better presented as $P_{ex}/P_t \,/\, P_{ty}/P_{tx}$ versus L/D as shown in Fig. 12d. In this figure the data are compared with the two-nozzle cluster data presented in Ref. 1. The line representing the four-nozzle cluster data (nozzle configuration C) does not increase as rapidly as the two-nozzle cluster data (Fig. 12d) with increasing L/D. No optimum L/D was determined for the four-nozzle configuration C.

4.3 MASS EJECTION FROM TEST CELL FOR VARIOUS EJECTOR-DIFFUSER CONFIGURATIONS

Reported in Ref. 1 is the P_c/P_t performance improvement of single- and two-nozzle ejector-diffuser configurations with mass ejected from the test cell by either one or two jet pumps. This work has been continued for different nozzle configurations and diffuser sizes and with steam and air as the ejector-diffuser driving fluids.

4.3.1 Single-Nozzle Configurations of Different A_{ne}/A^*

Presented in Fig. 6 is the performance for both air and steam used as ejector-diffuser nozzle driving fluids with and without ejected mass, W_b, from the test cell. The cell pressure ratio performance for either air or steam as the driving fluid, without ejected mass from the test cell (see configuration 2-B1), as shown in Fig. 6 is in good agreement with the data in Ref. 4 for the $A_{ne}/A^* = 18.00$ nozzle. With ejected mass from the test cell and air as the driving fluid, the P_c/P_t performance improvement was 2.17 for one jet pump and 2.62 for two jet pumps. This improvement was accomplished by ejecting $W_b/W_a = 0.146$ percent (W_a is the simulated rocket nozzle driving fluid weight flow). With steam as the driving fluid, the P_c/P_t performance improvement was 1.97 for one jet pump and 2.17 for two jet pumps, but the W_b/W_a ratio was not determined. The jet pump performance calibration with steam as the secondary fluid had not been made. Presented in Fig. 6 is the curve for one jet pump performance over a variation of exit pressure to breakdown. Breakdown P_{ex}/P_t was the same with or without ejected mass, as was shown in Ref. 1.

Figure 9 shows the performance for both nozzle configurations B3 and B4 driving diffuser configurations 2 and 3 with and without ejected mass. The P_c/P_t improvement by ejecting mass from the test cell as shown in Table 3 is as follows:

Configuration	A_d/A^*	One Jet Pump		Two Jet Pumps	
		$P_c/P_t \,/\, (P_c/P_t)'$	W_b/W_a, percent	$P_c/P_t \,/\, (P_c/P_t)'$	W_b/W_a, percent
2-B3	35.09	2.355	0.604	2.711	1.027
3-B3	60.43	1.948	0.153	2.029	0.279
2-B4	35.09	2.214	0.786	2.696	1.312
3-B4	60.43	1.735	0.510	2.048	1.030

The P_c/P_t improvement decreased for an increase in A_d/A^*. The use of one or two jet pumps for a given A_d/A^* did not appreciably affect

the P_c/P_t performance. Again breakdown occurred approximately at the same P_{ex}/P_t with or without ejected mass.

A comparison of the performance with ejected mass for various diffusers driven by nozzles with different A_{ne}/A^* is presented in Figs. 10a and b. The small area ratio nozzles have the higher P_c/P_t performance as a result of the large impingement angles even with ejected mass. A unique characteristic of the P_c/P_t performance with ejected mass is that the ratio of P_c/P_t does not vary with A_d/A^* as much as it does with no ejected mass. A limiting ejector-diffuser A_d/A^* exists for a particular jet pump at which no further improvement in P_c/P_t is possible. This is accomplished when the ejector-diffuser test cell pressure without ejected mass is equal to the jet pump no-secondary-flow cell pressure.

4.3.2 Two-Nozzle Configuration A

Both additional data and data from Ref. 1 for nozzle configuration A (two-nozzle cluster) driving different size diffusers with and without ejected mass are presented in Fig. 10c. This ejector-diffuser P_c/P_t performance with ejected mass shows an improvement by as much as 1/10 of P_c/P_t for the small A_d/A^* ejector-diffuser configurations.

It should be noted that, when mass is ejected from the cell, there is only a small change in P_c/P_t for a wide range of ejector-diffuser area ratios A_d/A^*. This almost invariant P_c/P_t with A_d/A^* performance illustrates the fact that the selection of a small diffuser when operated with ejected mass loses little in P_c/P_t performance. Since a small diffuser can operate at a higher exit pressure than a large one, the small diffuser is more desirable from the standpoint of extending the facility test range capability. The P_c/P_t performance for nozzle configuration A with one jet pump parallels that for the two jet pumps but at a higher P_c/P_t level by a factor of approximately 1.35.

4.3.3 Four-Nozzle Configuration C

Similar to Fig. 10c is Fig. 10d, which is the P_c/P_t performance of the four-nozzle cluster configuration C driving various sizes of diffusers with and without mass ejected from the test cell. Again the mass-ejected-from-the-test-cell performance curves are much less variant with A_d/A^* than the no-mass-ejected line. The ratio P_c/P_t for the smallest ejector-diffuser investigated was reduced by as much as 20.8 percent by ejecting mass from the test cell. This improvement decreased with increasing A_d/A^* as shown previously for the two-nozzle cluster in Fig. 10c. The curves representing mass ejected from the test cell by one and two jet pumps are shown in Fig. 10d to converge slightly for increasing A_d/A^*.

The one-jet-pump line is higher than the two-jet-pump line by a decreasing factor of 1.35 at the small A_d/A^* ejector-diffuser to 1.18 at the large A_d/A^* ejector-diffuser.

4.4 INFLUENCE OF DIFFUSER-TO-NOZZLE-EXIT AREA RATIO ON SECOND-THROAT PERFORMANCE WITH RESPECT TO NOZZLE-EXIT-TO-SECOND-THROAT SPACING AND SECOND-THROAT CONTRACTION RATIO

The understanding of the problems associated with the performance of ejector-diffusers is further complicated by the addition of a contraction known as a second throat. Such additional problems involved when adding a second throat are (1) the optimum spacing of the driving nozzle exit from the beginning of the second-throat contraction, (2) the limiting second-throat contraction area ratio, A_{st}/A_d, (3) the effects of diffuser-to-nozzle-exit area ratio, A_d/A_{ne}, on starting at various contraction area ratios, A_{st}/A_d, (4) the optimum length of the constant-area second-throat duct, and possibly (5) the limiting or optimum magnitude of the angle of the second-throat transition section. Data from the study of problems 1, 2, and 3 are presented in this report. Problems 1, 2, and 4 are discussed in Refs. 1 and 2. A second throat is added to allow started ejector-diffuser operation to continue at a higher exit pressure than is possible with only a constant-area diffuser. This ability to operate at a higher exit pressure makes the effort worthwhile for the development of a feasible second-throat configuration.

4.4.1 Single-Nozzle-Driven, Second-Throat, Ejector-Diffuser Configurations

The results of the single-nozzle configuration B3 (Table 1) driving the second-throat diffusers S3a, b, and c (Table 2) along with the constant-area diffuser configuration 3 is shown in Fig. 13a. Neither the S3a-B3 nor the S3b-B3 (A_{st}/A_d = 0.4298 and 0.5672, respectively) ejector-diffuser configuration would start and pump the minimum P_c/P_t obtained by the constant-area ejector-diffuser configuration 3-B3. For this report, a second-throat ejector-diffuser is considered started when the second-throat minimum P_c/P_t is equal to that obtained when there is no second throat (straight diffuser). The contraction ratio, A_{st}/A_d = 0.4298, for S3a-B3 is approximately equal to the limiting contraction ratio for the one-dimensional duct Mach number, M_d = 6.18, based on A_d/A^* as shown in Fig. 9 of Ref. 2. The curve of limiting contraction in Ref. 2 indicates that this S3a-B3 configuration should start. According to Ref. 2, configuration S3b-B3 (A_{st}/A_d = 0.5672) is well within the start and operating region, but this S3b-B3 configuration also failed to start. The momentum or a force balance analysis presented in Ref. 11 predicts that the S3a-B3 and S3b-B3 configurations will not start and pump the straight ejector-diffuser minimum P_c/P_t. The contraction was too small for both S3a-B3

and S3b-B3 configurations. The P_c/P_t performance for the S3a-B3 and S3b-B3 was obtained for an optimum location of the nozzle exit from the beginning of the second throat. Positions less than or greater than the optimum shown in Table 4 and Fig. 13a would cause P_c/P_t to increase.

When the contraction ratio, A_{st}/A_d, was increased from 0.5672 to 0.6479 (from S3b-B3 to S3c-B3), the ejector-diffuser started and pumped approximately the minimum P_c/P_t obtained for the straight ejector-diffuser configuration 3-B3 as shown in Fig. 13a. Configuration S3c-B3 was predicted by the method of Ref. 11 to start and pump the minimum no second-throat P_c/P_t. The A_{st}/A_d = 0.6479 for S3c-B3 configuration is greater than the normal shock contraction ratio, $(A_{st}/A_d)_{ns}$ = 0.6316, for the one-dimensional duct Mach number, M_d = 6.18, based on A_d/A^*. In order to keep P_c a minimum, the minimum distance between the second throat and the nozzle exit was 4.62 in., whereas the maximum distance before the diffuser would break down was 5.62 in. The distance of the nozzle exit from the beginning of the second throat could be varied only by a maximum of 1.0 in. and still hold P_c/P_t constant at the minimum value pumped by the straight ejector-diffuser configuration 3-B3. The point of breakdown and start near the two extreme positions occurred at different P_{ex}/P_t ratios. The P_{ex}/P_t for the near minimum position of the nozzle exit to the beginning of the second throat (4.75 in.) was 0.0156, which was lower than that obtained for the straight diffuser configuration (P_{ex}/P_t = 0.0190). The near maximum position of the beginning of the second throat from the nozzle exit (5.19 in.) resulted in start and breakdown P_{ex}/P_t of 0.01958. This was practically the same as the P_{ex}/P_t value (0.0190) obtained for the straight diffuser configuration 3-B3. It is not known what performance would have resulted if additional contractions between A_{st}/A_d = 0.5672 and 0.6479 had been investigated. The nozzle exit Mach number, M_{ne}, based on the nozzle area ratio, A_{ne}/A^*, for nozzle configuration B3 is 2.92. The ratio of duct-to-nozzle exit area, A_d/A_{ne}, was 15.44. The A_d/A_{ne} ratios from the Refs. 2 and 12 investigations were equal to approximately 2 or less. This indicates that the limiting contraction ratio is related to A_d/A_{ne}.

The scarf nozzle, configuration B4, was used as the driving nozzle for the second-throat diffuser configurations S3b and S3c. Unlike the performance of diffuser S3c configuration driven by nozzle configuration B3, the S3c diffuser did not start when driven by nozzle configuration B4. The average M_{ne} based on A_{ne}/A^* for nozzle configuration B4 (Table 1) was 2.69 as shown in Table 4, whereas the M_d based on the constant A_d/A^* did not change from that of S3c-B3 configuration. The decreased average nozzle exit area of the scarf nozzle increased the A_d/A_{ne} from 15.44 for S3c-B3 to 19.18 for S3c-B4. Since A_d/A^* did not change and the diffuser was started for S3c-B3 configuration, the

decreased nozzle exit area is considered responsible for the S3c-B4 configuration not starting. The limiting contraction ratio, A_{st}/A_d, appeared to increase as A_d/A_{ne} increased. The fact that this B4 nozzle configuration was a scarf nozzle could have some conclusive influence on the limiting contraction ratio of the second throat. Even the minimum obtainable P_c/P_t for the $A_{st}/A_d = 0.5672$ (S3b configuration) was higher for the B4 nozzle configuration (Fig. 13b) than the P_c/P_t obtained for the B3 nozzle configuration (Fig. 13a).

The single-nozzle configuration D (Fig. 2d and Table 1) was used to drive the S3b and S3c second-throat diffusers (Fig. 2b and Table 1) and the straight cylindrical diffuser configuration 3 (Fig. 4a). Second-throat diffuser configuration S3c, which has an $A_{st}/A_d = 0.5672$ when driven by nozzle configuration D, did not pump the minimum P_c/P_t that was pumped by the straight cylindrical ejector-diffuser configuration 3-D as shown in Fig. 13c. Reference 11 predicts that second-throat configuration S3b-D should have pumped the same minimum P_c/P_t as the straight cylindrical configuration 3-D. Actually, P_c/P_t for configuration S3b-D is approximately 24 percent higher than the P_c/P_t obtained by the straight cylindrical configuration. The contraction for configuration S3b-D ($A_{st}/A_d = 0.5672$) is either very near the minimum contraction for starting or small leakage into the test cell existed. When the nozzle exit was 4.81 in. from the beginning of the second throat, a large difference in P_{ex}/P_t was obtained ($P_{ex}/P_t = 0.0229$ at breakdown and 0.00625 at start). Breakdown and start P_{ex}/P_t were equal when the second throat was moved 1.5 in. farther downstream of the nozzle exit, giving a total spacing of 6.31 in. The $A_{st}/A_d = 0.6479$ configuration S3c-D ejector-diffuser pumped P_c/P_t (0.000275) slightly below the straight cylindrical ejector-diffuser P_c/P_t (0.000319). Again a wide variation of P_{ex}/P_t at breakdown and start was experienced when the nozzle exit was 4.75 in. upstream of the beginning of the second throat. However, when the position of the nozzle with respect to the second throat was increased from 4.75 to 5.00 in., no difference in P_{ex}/P_t for start and breakdown was detected as shown in Fig. 13c. A small increase was detected in P_{ex}/P_t (0.0211 to 0.0222) when the position of the beginning of the second throat from the nozzle exit was increased to 9.25 in. A quite large difference in start and breakdown P_{ex}/P_t (0.0107 at start to 0.0170 at breakdown) existed for configuration 3-D (straight cylindrical ejector-diffuser configuration). The A_d/A_{ne} for the S3b-D and S3c-D was 6.43. The A_d/A^* was not much greater for S3b-D and S3c-D configurations (67.58) than it was for the S3a-B3, S3b-B3, and S3c-B3 configurations (60.43). The greatest difference in the configurations is in the A_d/A_{ne}.

4.4.2 Two-Nozzle-Driven, Second-Throat, Ejector-Diffuser Configuration

The two-nozzle configuration A (Fig. 2a and Table 1) was used to drive the S3b diffuser (Fig. 4b and Table 2) where $A_{st}/A_d = 0.5672$. The position of the beginning of the second throat was varied from 5.16 to 8.38 in. from the nozzle exit without affecting the minimum P_c. The positioning did affect P_{ex}/P_t at breakdown. As shown in Fig. 13d for the 5.81 in. position of the second throat, P_{ex}/P_t at breakdown was lower than that obtained for the straight cylindrical ejector-diffuser configuration 3-A, but when the position of the second throat was changed to 5.84 in., the breakdown P_{ex}/P_t was greater than that of the straight cylindrical diffuser. This positioning was very critical. The diffuser-to-nozzle exit area ratio, $A_d/A_{ne} = 6.28$, is larger for configuration S3b-A than for those configurations tested in Refs. 2 and 12.

4.4.3 Four-Nozzle-Driven, Second-Throat, Ejector-Diffuser Configuration

The four-nozzle configuration C (Fig. 2c and Table 1) was used to drive the S3b and S3c diffusers (Fig. 4b and Table 2). The S3b-C ejector-diffuser configuration did not start and pump the minimum P_c/P_t pumped by the straight cylindrical configuration 3-C as presented in Fig. 13e. According to Ref. 2 (which presents only data for single nozzles), this S3b-C configuration should start since the contraction ratio, $A_{st}/A_d = 0.5672$, was well above the limiting contraction for the one-dimensional duct $M_d = 5.59$ based on A_d/A^*. Reference 11 predicts from a momentum or force balance analysis that ejector-diffuser configuration S3b-C should not start. The diffuser-to-nozzle exit area ratio for configuration S3b-C, $A_d/A_{ne} = 9.57$, was higher than the $A_d/A_{ne} = 6.28$ for the two-nozzle configuration S3b-A presented in Fig. 13d. Again this indicates that the limiting contraction ratio, A_{st}/A_d, increases with increasing A_d/A_{ne} as shown for the previous configurations discussed. When the nozzle exit was 4.50 in. from the beginning of the second throat, the minimum P_c/P_t of 0.00255 was obtained, which is higher than the minimum obtained for a straight cylindrical diffuser ($P_c/P_t = 0.00146$).

Ejector-diffuser configuration S3c-C did start. This configuration had an $A_{st}/A_d = 0.6479$, which was near the normal shock contraction ratio, $(A_{st}/A_d)_{ns} = 0.6388$. As shown in Fig. 13e at the 4.81-in. position of the nozzle exit, the same peculiar start and breakdown characteristic was evident as was experienced previously with the single- and two-nozzle configurations. This was the minimum position from the beginning of the second throat for minimum P_c. Breakdown and start occurred at a lower P_{ex}/P_t value than was obtained for the 3-C straight cylindrical diffuser configuration. When the position of the second throat

from the nozzle exit was increased from 4.81 to 5.44 in., start and breakdown occurred at the same P_{ex}/P_t = 0.0284 value, which was greater than the start and breakdown P_{ex}/P_t = 0.0256 value obtained for the straight cylindrical configuration 3-C. The position of the second throat was moved from 4.81 to 5.94 in. from the nozzle exit while P_{ex}/P_t was low (0.00445) before breakdown occurred as shown in Fig. 13e, but for restart the position of the second throat was 5.44 in. This gives a total of 0.63 in. between minimum and maximum positioning of the second throat without affecting P_c. Again the spacing of the second throat from the beginning of the nozzle exit was very critical, and from little to no improvement in P_{ex}/P_t was obtained at the second-throat contraction ratios tested.

5.0 SUMMARY OF RESULTS

The results of a model investigation of the influence of pertinent parameters on ejector-diffuser performance with and without ejected mass are summarized as follows:

1. The cell-to-nozzle total pressure ratio, P_c/P_t, is affected by varying the nozzle area ratio, A_{ne}/A^*, for a constant diffuser-to-nozzle throat area ratio. An increase in P_c/P_t by an average factor of approximately 1.68 was obtained when the driving nozzle A_{ne}/A^* was decreased from 18.00 to 5.00 by cutting off the exit and by using different size diffusers. The start and breakdown pressure ratio was decreased by as much as 8 percent for small diffusers (4.026-in. diam), whereas no essential difference was experienced for larger diffusers (8.092-in. diam) when the nozzle area ratio was decreased from 18.00 to 5.00. The effect of decreasing the nozzle area ratio by cutting the nozzle exit off at an angle other than perpendicular to the nozzle centerline resulted in a similar change in performance.

2. A bend in a constant-area diffuser affects the ejector-diffuser performance only in breakdown and start pressure ratio, P_{ex}/P_t, as a result of a change in the effective diffuser length-to-diameter ratio (L/D upstream of bend). A diffuser with a large gradual turn (such as configuration 6-B3) performed more like a long straight diffuser (high $P_{ex}/P_t \,/\, P_{ty}/P_{tx}$ = 0.6892 for effective L/D = 2.59), whereas a diffuser with a short sudden turn (such as configuration 7-B3) performed like a short straight diffuser (low $P_{ex}/P_t \,/\, P_{ty}/P_{tx}$ = 0.6503 for effective L/D = 3.27) depending on the length of the straight section upstream of the bend.

3. For essentially the same half-angle and for any particular diffuser-to-nozzle throat area ratio, A_d/A^*, the larger the diffuser driving nozzle area ratio the lower the P_c/P_t will be regardless of whether one-, two-, or four-nozzle clusters are used.

4. A unique characteristic of ejected mass from the test cell is that the cell pressure ratio, P_c/P_t, does not vary with A_d/A^* as much as it does when no mass is ejected. This enables one to select a smaller diffuser which has a higher start and breakdown pressure ratio, P_{ex}/P_t, thus extending the facility test range capability.

5. The limiting second-throat contraction ratio, A_{st}/A_d, increased with increasing ratio of the diffuser-to-nozzle exit area, A_d/A_{ne}, regardless of the number of diffuser driving nozzles used (one, two, or four). When the A_d/A_{ne} is equal to or greater than 6, the spacing of the second throat with respect to the nozzle exit was noted to become very critical as far as breakdown and start pressure ratio performance improvement is concerned. However, spacing is critical any time the limiting contraction ratio, A_{st}/A_d, is approached. A second throat for such a configuration with large A_d/A_{ne} may not give any improvement in P_{ex}/P_t.

REFERENCES

1. Hale, James W. "Investigation of Two-Nozzle-Cluster Diffuser-Ejector with and without Ejected Mass." AEDC-TDR-63-130, November 1963.

2. Bauer, R. C. and German, R. C. "The Effects of Second-Throat Geometry on the Performance of Ejectors without Induced Flow." AEDC-TN-61-133, November 1961.

3. Wang, C. J., Paterson, J. B., and Anderson, R. "Gas Flow Tables." GM-TR-154, March 1957.

4. Barton, D. L. and Taylor, D. "An Investigation of Ejectors without Induced Flow." AEDC-TN-59-145, December 1959.

5. Hale, James W. "Comparison of Diffuser-Ejector Performance with Five Different Driving Fluids." AEDC-TDR-63-207, October 1963.

6. Gooderum, Paul B., Wood, George P., and Brevoort, Maurice J. "Investigation with an Interferometer of the Turbulent Mixing of a Free Supersonic Jet." NACA Report 963, 1950.

7. Korst, H. H., Page, R. H., and Childs, M. E. "A Theory for Base Pressures in Transonic and Supersonic Flow." University of Illinois, ME-TN-392-2, March 1955.

8. Latvala, E. K. "Spreading of Rocket Exhaust Jets at High Altitudes." AEDC-TR-59-11, June 1959.

9. Sivo, Joseph N., Meyer, Carl L., and Peters, Daniel J. "Experimental Evaluation of Rocket Exhaust Diffusers for Altitude Simulation." NASA TN D-298, July 1960.

10. Aerojet-General Corporation. "Analytical and Experimental Evaluation of Ejectors with 90-deg Turns." Report No. 2403, November 1962.

11. Panesci, J. H. and German, R. C. "An Analysis of Second-Throat Diffuser Performance for Zero-Secondary-Flow Ejector Systems." AEDC-TDR-63-249, December 1963.

12. Jones, W. L., Price, H. G., and Lorenzo, C. F. "Experimental Study of Zero-Flow Ejectors Using Gaseous Nitrogen." NASA TN D-203, March 1960.

TABLE 1

DESCRIPTION OF NOZZLE CONFIGURATIONS

Nozzle Configuration (See Fig. 2)	Nozzle Number (See Fig. 3)	Nozzle Geometry			
		d*, in.	d_{ne}, in.	θ_n, deg	A_{ne}/A^*
A[1]	-2[1]	0.51	1.750	13.254	11.77
	-3[1]	0.50			12.25
B1	1	0.471	2.000	18	18.00
B2	2	0.471	1.053	18	5.00
B3	3	0.790	1.563	10	3.914
B4	4	0.790	Scarf[2]	10	3.147[3]
C	5	0.489	0.980	15	4.016
	6	0.490	1.005	15	4.207
	7	0.4885	0.995	15	4.149
	8	0.4885	0.990	15	4.107
D	9	0.747	2.421	9.00	10.51

[1]Nozzle details given in Fig. 3 of Ref. 1

[2]Nozzle exit cut at an angle to the centerline (1.218-in. minimum diameter and 1.563-in. maximum diameter.

[3]Average nozzle exit area based on the 1.218-in. minimum diameter and 1.563-in. maximum diameter.

TABLE 2

DESCRIPTION OF DIFFUSER CONFIGURATIONS

Configuration Number	Type	Detail Dimensions				Area	
		L[1], in.	ℓ, in.	D, in.	d, in.	A_d, in.^{2}	A_{st}, in.^{2}
1	Straight Cylindrical	24.00	—	4.026	—	12.73	—
2	Straight Cylindrical	25.50	—	4.680	—	17.20	—
3	Straight Cylindrical	24.00	—	6.141	—	29.62	—
S3a	Straight Cylindrical with Second-Throat 15-deg Transition Section	Varied	20.30	6.141	4.026	29.62	12.73
S3b	Straight Cylindrical with Second-Throat 15-deg Transition Section	Varied	21.42	6.141	4.625	29.62	16.80
S3c	Straight Cylindrical with Second-Throat 15-deg Transition Section	Varied	22.02	6.141	4.943	29.62	19.19
4	Straight Cylindrical	31.438	—	8.092	—	51.43	—
5	Straight Cylindrical	46.50	—	10.020	—	78.85	—
6	Cylindrical with 90-deg Long Radius Elbow	15.50[2]	—	5.763	—	26.08	—
7	Cylindrical with 60-deg Miter Bend	15.75[2]	—	4.647	—	16.96	—
8	Cylindrical with 60-deg Miter Bend	11.43[2]	—	5.763	—	26.08	—

[1]Overall length of diffuser or distance between diffuser inlet and beginning of second throat.

[2]Length of diffuser before bend.

TABLE 3

SUMMARY OF CONSTANT-AREA DIFFUSER TEST DATA

Run No.	Test Config. Code	Diffuser		Area Ratio and Mach No.				Without Ejected Mass			With Ejected Mass			Starting, Operating Pressure Ratios			Nozzle Driving Fluid	
		Diam, D, in.	Ratio, L/D[6]	A_{ne}/A^*	M_{ne}	A_d/A^*	M_d	$(P_c/P_t)_{act} \times 10^3$	$(P_c/P_t)_{isen} \times 10^3$	$\frac{(P_c/P_t)_{act}}{(P_c/P_t)_{isen}}$	$(P_c/P_t)'_{act} \times 10^3$	W_b/W_a, percent	$\frac{(P_c/P_t)_{act}}{(P_c/P_t)'_{act}}$	P_{ex}/P_t	P_{ty}/P_{tx}	$\frac{P_{ex}/P_t}{P_{ty}/P_{tx}}$	P_t, psia	T_t, °R
29	1-B1	4.026	5.37	18.00	4.59	73.07	6.46	0.480	0.4006	1.198	0.1703	0.640	2.824	0.0168[1]	0.0217	0.7738	312	512
22	2-B1	4.680	4.04	18.00	4.59	98.74	6.92	0.330	0.2598	1.270	0.1523	0.146	2.171	0.0129[1]	0.0161	0.8012	307	520
											0.1264	-	2.619	0.0114[2]	0.0161	0.7081		
46	4-B1	8.092	3.59	18.00	4.59	295.22	8.80	0.096	0.0549	1.749	-	-	-	0.0035	0.0055	0.6364	359	519
42	5-B1	10.02	4.40	18.00	4.59	452.66	9.65	0.082	0.0299	2.742	-	-	-	0.0022	0.0036	0.6111	348	514
25	6-B1	5.763	2.28	18.00	4.59	140.74	7.59	0.190	0.1439	1.320	0.1253	-	1.520	0.0072	0.0107	0.6729	331	520
49	1-B2	4.026	5.73	5.00	3.18	73.07	6.46	0.715	0.4006	1.785	0.3643	0.428	1.964	0.0155	0.0217	0.7143	348	525
											0.3194	-	2.241					
50	3-B2	8	3.76	5.00	3.18	170.03	7.81	0.320	0.1197	2.673	0.2154	-	1.488	0.0065	0.0095	0.6842	346	525
48	4-B2	8.092	3.77	5.00	3.18	295.22	8.80	0.178	0.0549	3.242	0.1574	0.117	1.134	0.0035	0.0055	0.6364	342	527
17	2-B3	4.680	5.33	3.914	2.92	35.09	5.43	1.540	1.1910	1.326	0.6543	0.604	2.355	0.0326	0.0446	0.7309	309	510
											0.5684	1.027	2.711					
1	3-B3	6.141	3.82	3.914	2.92	60.43	6.18	0.830	0.5278	1.573	0.4263	0.153	1.948	0.0190	0.0282	0.7252	302	518
											0.4094	0.279	2.029					
23	6-B3	5.763	2.59	3.914	2.92	53.22	6.00	0.920	0.6334	1.452	0.1393	0.352	2.096	0.0204	0.0296	0.6892	322	511
39	7-B3	4.647	3.27	3.914	2.92	34.60	5.42	1.650	1.1740	1.405	-	-	-	0.0292	0.0449	0.6503	297	486
38	8-B3	5.763	1.69	3.914	2.92	53.22	6.00	0.925	0.6334	1.460	-	-	-	0.0158	0.0296	0.5338	291	496
18	2-B4	4.680	5.45	3.1475	2.69	35.09	5.43	1.860	1.1610	1.602	0.8403	0.786	2.214	0.0318	0.0446	0.7130	305	510
											0.6904	1.312	2.696					
11	3-B4	6.141	3.91	3.1475	2.69	60.43	6.18	1.020	0.5278	1.932	0.5883	0.510	1.735	0.0178	0.0282	0.6794	309	513
											0.4984	1.030	2.048					
24	6-B4	5.763	2.69	3.1475	2.69	53.22	6.00	1.050	0.6334	1.657	0.6033	0.508	1.741	0.0192	0.0296	0.6486	271	509
41	7-B4	4.647	3.39	3.1475	2.69	34.60	5.42	1.830	1.1740	1.559	0.8403	0.780	2.179	0.0271	0.0449	0.6036	296	502
37	8-B4	5.763	1.98	3.1475	2.69	53.22	6.00	1.100	0.6334	1.736	-	-	-	0.0140	0.0286	0.4730	282	488

NOTES:
1. P_{ex}/P_t at breakdown
2. P_{ex}/P_t at start
3. One jet pump
4. Two jet pumps
5. Based on average nozzle exit area
6. Length L is the distance from the nozzle exit to the diffuser exit or to the bend in the diffuser

TABLE 3 (Concluded)

Run No.	Test Config. Code	Diffuser		Area Ratio and Mach No.				Without Ejected Mass			With Ejected Mass			Starting, Operating Pressure Ratios			Nozzle Driving Fluid	
		Diam, D, in.	Ratio, L/D_6	A_{ne}/A^*	M_{ne}	A_d/A^*	M_d	$(P_c/P_t)_{act}$ x 10^3	$(P_c/P_t)_{isen}$ x 10^3	$\frac{(P_c/P_t)_{act}}{(P_c/P_t)_{isen}}$	$(P_c/P_t)'_{act}$ x 10^3	W_b/W_a, percent	$\frac{(P_c/P_t)_{act}}{(P_c/P_t)'_{act}}$	P_{ex}/P_t	P_{ty}/P_{tx}	$\frac{P_{ex}/P_t}{P_{ty}/P_{tx}}$	P_t, psia	T_t, °R
	1d-A	4.680	5.45	12.01	4.13	42.94	5.70	1.369			0.400_3	0.471	3.423	0.0295	0.0385	0.808	403	471
											0.300_4	0.628	4.563					
Ref. 1	1b-A	6.065	3.96	12.01	4.13	72.11	6.44	0.662	0.409	1.619	0.385_3	0.377	1.719	0.0171	0.0220	0.777	381	478
Data	4a-A	2.469	10.68	12.01	4.13	23.36	4.92	2.076	2.087	0.995	0.440_3	0.483	4.718	0.0556	0.0659	0.844	308	467
											0.321_4	0.617	6.467					
	5-A	2.065	13.77	12.01	4.13	16.72	4.51	3.335	3.407	0.979	0.494_3	0.481	6.751	0.0723	0.0909	0.796	270	457
											0.338_4	0.423	9.926					
28	6-A	5.763	2.95	12.01	4.13	65.11	6.29	0.690	0.4731	1.458	0.347_3	0.308	1.988	0.0145	0.0243	0.5967	335	512
4	3-A	6.141	4.15	12.01	4.13	73.93	6.47	0.635	0.3968	1.600	0.352_3	0.370	1.804	0.0175	0.0216	0.8102	362	507
											0.267_4	0.482	2.378					
44	4-A	8.092	4.08	12.01	4.13	128.37	7.34	0.338	0.1785	1.894	0.257_4	0.110	1.315	0.0079	0.0125	0.6320	293	487
43	5-A	10.02	4.80	12.01	4.13	196.82	8.06	0.195	0.0976	1.998	-	-	-	0.0052	0.0082	0.6341	282	501
33	1-C	4.026	5.81	4.12	2.97	16.85	4.53	3.600	3.329	1.081	0.966_3	0.563	3.727	0.0650	0.0895	0.7263	216	497
											0.752_4	0.820	4.787					
19	2-C	4.680	5.32	4.12	2.97	22.90	4.89	2.660	2.151	1.237	1.027_3	0.638	3.590	0.0474	0.0672	0.7054	208	502
											0.718_4	0.783	3.705					
27	6-C	5.763	2.56	4.12	2.97	34.72	5.43	1.610	1.174	1.371	0.857_3	0.568	1.879	0.0287	0.0449	0.6392	300	507
12	3-C	6.141	3.81	4.12	2.97	39.43	5.59	1.460	0.9748	1.498	0.817_3	0.525	1.787	0.0256	0.0387	0.6448	307	513
											0.581_4	0.670	2.513					
45	4-C	8.092	3.81	4.12	2.97	68.46	6.36	0.920	0.4416	2.083	0.683_3	0.413	1.347	0.0157	0.0232	0.6767	334	486
											0.558_4	0.589	1.649					
43	5-C	10.02	4.58	4.12	2.97	104.97	7.01	0.600	0.2394	2.506	0.506_3	0.184	1.181	0.0100	0.0153	0.6536	310	491
											0.432_4	0.420	1.389					
18A-3	3-D	6.141	3.76	10.51	3.98	67.58	6.35	0.329	0.446	0.738	-	-	-	0.0170_1	0.0234	0.7265	302	507
														0.0107_2	0.0234	0.4573		
									(Steam Driving Fluid)									
22	2-B1	4.680	4.94	18.00	4.11	98.74	5.79	0.850	0.4160	2.043	0.432_3	-	1.968	0.147_1	0.0172	0.8547	192	790
											0.392_4	-	2.168	0.128_2	0.0172	0.7442		

NOTES:
1. P_{ex}/P_t at breakdown
2. P_{ex}/P_t at start
3. One jet pump
4. Two jet pumps
5. Based on average nozzle exit area
6. Length L is the distance from the nozzle exit to the diffuser exit or to the bend in the diffuser

TABLE 4

SUMMARY OF SECOND-THROAT DIFFUSER TEST DATA

Run No.	Test Config. Code	Capture Duct			Second-Throat Duct		Area Ratio and Mach No.				Contraction Ratio			Cell Pressure Ratio			Starting, Operating Pressure Ratios			Nozzle Driving Fluid	
		Diam, D, in.	Z, in.	X, in.	Diam, d, in.	Ratio, ℓ/d	A_{ne}/A^*	M_{ne}	A_d/A^*	M_d	$(A_{st}/A_d)_{act}$	$(A_{st}/A_d)_{ns}$	$\frac{(A_{st}/A_d)_{act}}{(A_{st}/A_d)_{ns}}$	$(P_c/P_t)_{act}$ x 10^3	$(P_c/P_t)_{isen}$ x 10^3	$\frac{(P_c/P_t)_{act}}{(P_c/P_t)_{isen}}$	P_{ex}/P_t	P_{ty}/P_{tx}	$\frac{P_{ex}/P_t}{P_{ty}/P_{tx}}$	P_t, psia	T_t, °R
2 & 3	S3a-B3	6.141	-0.56	2.03	4.026	5.043	3.914	2.92	60.43	6.18	0.4208	0.6316	0.6805	2.696	0.5278	5.108	-	0.0262	-	307	515
6	S3b-B3	6.141	-0.56	4.56	4.625	4.632	3.914	2.92	60.43	6.18	0.5672	0.6316	0.8980	1.988	0.5278	3.767	-	0.0262	-	270	512
16	S3c-B3	6.141	-0.56	4.75 →	4.943	4.454	3.914	2.92	60.43	6.18	0.6479	0.6316	1.0258	0.870	0.5278	1.648	0.0156 →	0.0262	0.5954 →	285	506
				5.19	4.943	4.454	3.914	2.92	60.43	6.18	0.6479	0.6316	1.0258				0.0196	0.0262	0.7481	285	506
10	S3b-B4	6.14	-0.56	3.06	4.625	4.632	3.147[3]	2.69	60.43	6.18	0.5672	0.6316	0.8980	2.093	0.5278	5.671	-	0.0262	-	166	524
13	S3c-B4	6.141	-0.56	4.44	4.943	4.454	3.147[3]	2.69	60.43	6.18	0.6479	0.6316	1.0258	2.502	0.5278	4.740	-	0.0262	-	300	513
8	S3b-D	6.141	-2.94	4.81	4.625	4.632	10.51	3.98	67.58	6.35	0.5672	0.6324	0.8969	0.426	0.4460	0.955	0.0229[1]	0.0234	0.9786	308	512
9	S3b-D	6.141	-2.94	4.81	4.625	4.632	10.51	3.98	67.58	6.35	0.5672	0.6324	0.8969	0.446	0.4460	1.000	0.0063[1]	0.0234	0.2692	308	508
3	S3b-D	6.141	-2.94	6.31	4.625	4.632	10.51	3.98	67.58	6.35	0.5672	0.6324	0.8969	0.446	0.4460	1.000	0.0238	0.0234	1.0171	308	505
17A-2	S3c-D	6.141	-0.91	4.75	4.943	4.454	10.51	3.98	67.58	6.35	0.6479	0.6324	1.0245	0.275	0.4460	0.617	0.0211[1]	0.0234	0.9017	300	501
17A-2	S3c-D	6.141	-0.91	5.00	4.943	4.454	10.51	3.98	67.58	6.35	0.6479	0.6324	1.0245	0.275	0.4460	0.617	0.00542[2]	0.0234	0.2308	300	501
17A-2	S3c-D	6.141	-0.91	5.25	4.943	4.454	10.51	3.98	67.58	6.35	0.6479	0.6324	1.0245	0.275	0.4460	0.617	0.0206	0.0234	0.8803	297	501
																	0.0222	0.0234	0.9487	297	501
5	S3b-A	6.141	+1.50	5.81	4.625	4.632	12.01	4.13	73.93	6.47	0.5672	0.6262	0.9058	0.630	0.3968	1.613	0.0105	0.0216	0.4861	365	508
5	S3b-A	6.141	+1.50	5.84	4.625	4.632	12.01	4.13	73.93	6.47	0.5672	0.6263	0.9058	0.630	0.3968	1.613	0.0156	0.0216	0.7222	361	508
7	S3b-C	6.141	-0.50	4.50	4.625	4.632	4.12	2.97	39.43	5.59	0.5672	0.6388	0.8879	2.560	0.9748	2.626	0.0250	0.0397	0.6297	240	507
15	S3c-C	6.141	-0.50	4.81	4.943	4.454	4.12	2.97	39.43	5.59	0.6479	0.6388	1.0142	1.456	0.9748	1.494	0.0160[1]	0.0397	0.4030	296	508
15	S3c-C	6.141	-0.50	4.81	4.943	4.454	4.12	2.97	39.43	5.59	0.6479	0.6388	1.0142	1.451	0.9748	1.489	0.0110[2]	0.0397	0.2771	293	508
15	S3c-C	6.141	-0.50	5.44	4.943	4.454	4.12	2.97	39.43	5.59	0.6479	0.6388	1.0142	1.445	0.9748	1.482	0.0281	0.0397	0.7078	267	508
15	S3c-C	6.141	-0.50	4.81 →	4.943	4.454	4.12	2.97	39.43	5.59	0.6479	0.6388	1.0142	1.451 →	0.9748	1.489 →	-	0.0397	-	293	508
				5.94										2.164	0.9748	2.220	-	0.0397	-	292	508

NOTE: [1] P_{ex}/P_t at Breakdown [2] P_{ex}/P_t at Start [3] Based on Average Nozzle Exit Area

BLANK PAGE

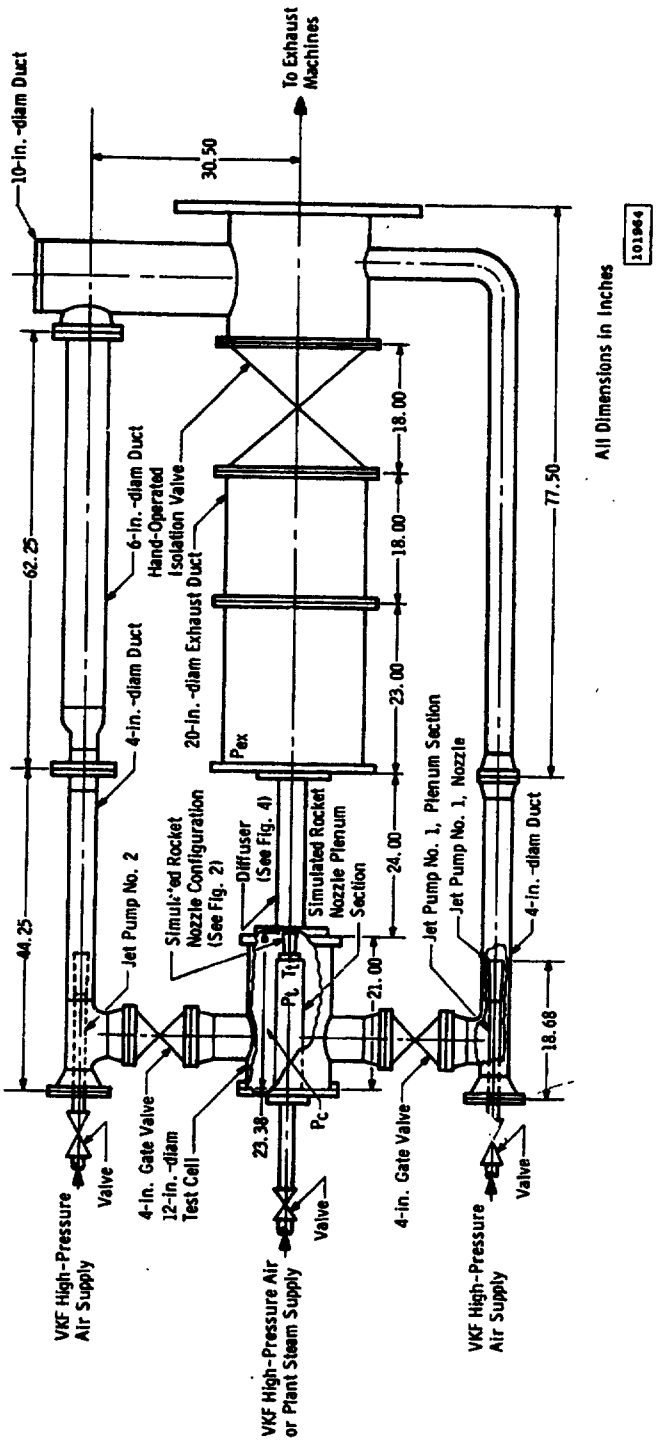

a. Straight and Second-Throat Cylindrical Diffuser Configuration Installation

Fig. 1 R-2D Test Installation

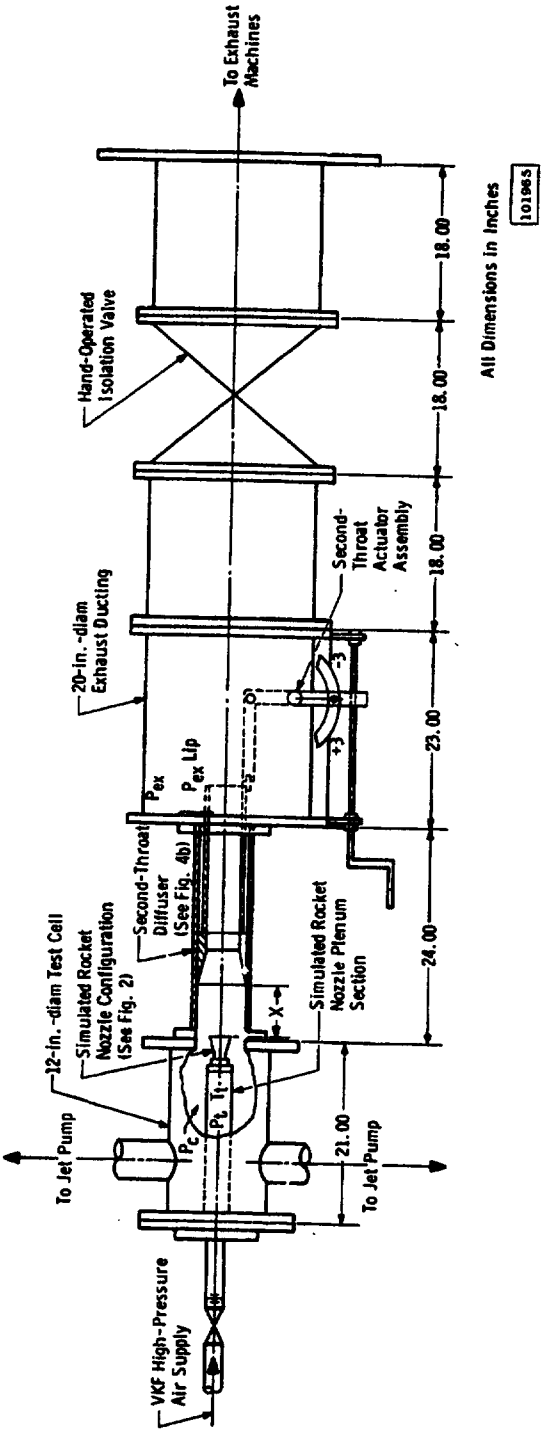

b. Second-Throat Cylindrical Diffuser Configuration Installation

Fig. 1 Continued

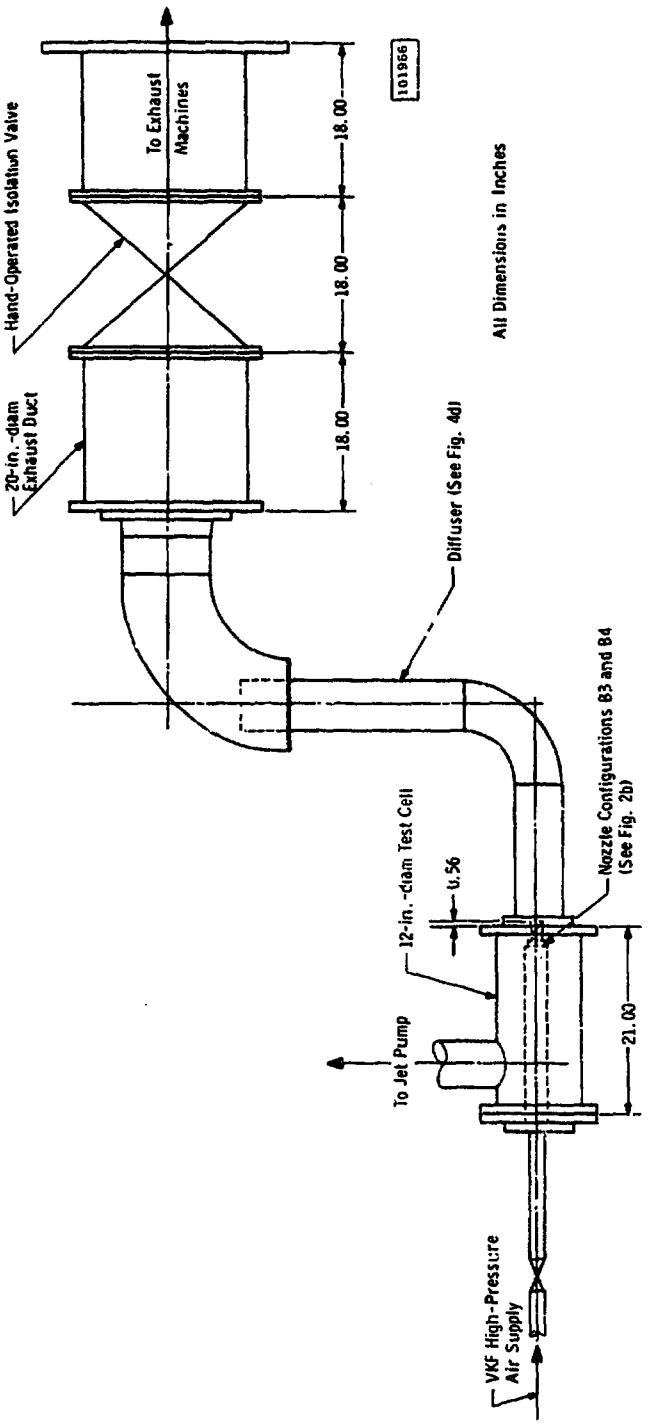

c. Diffuser Configuration 6 Installation

Fig. 1 Continued

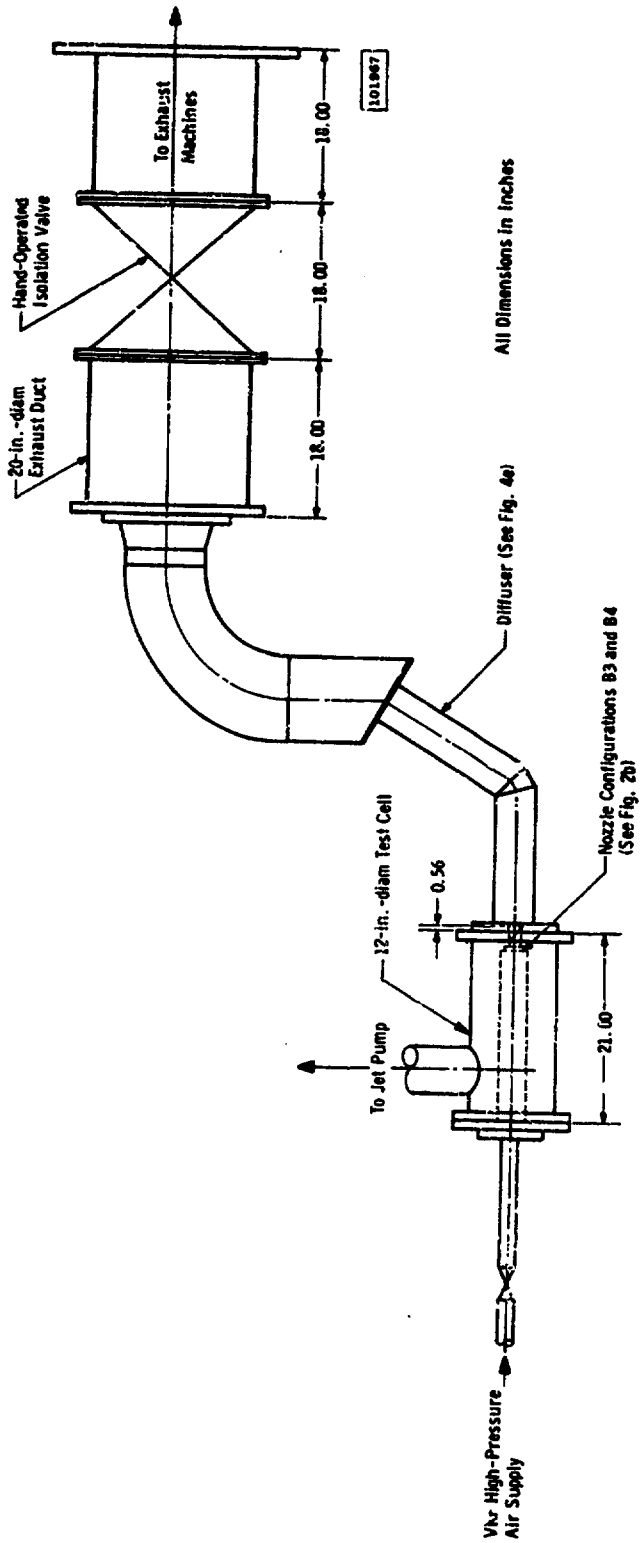

d. Diffuser Configuration 7 Installation

Fig. 1 Continued

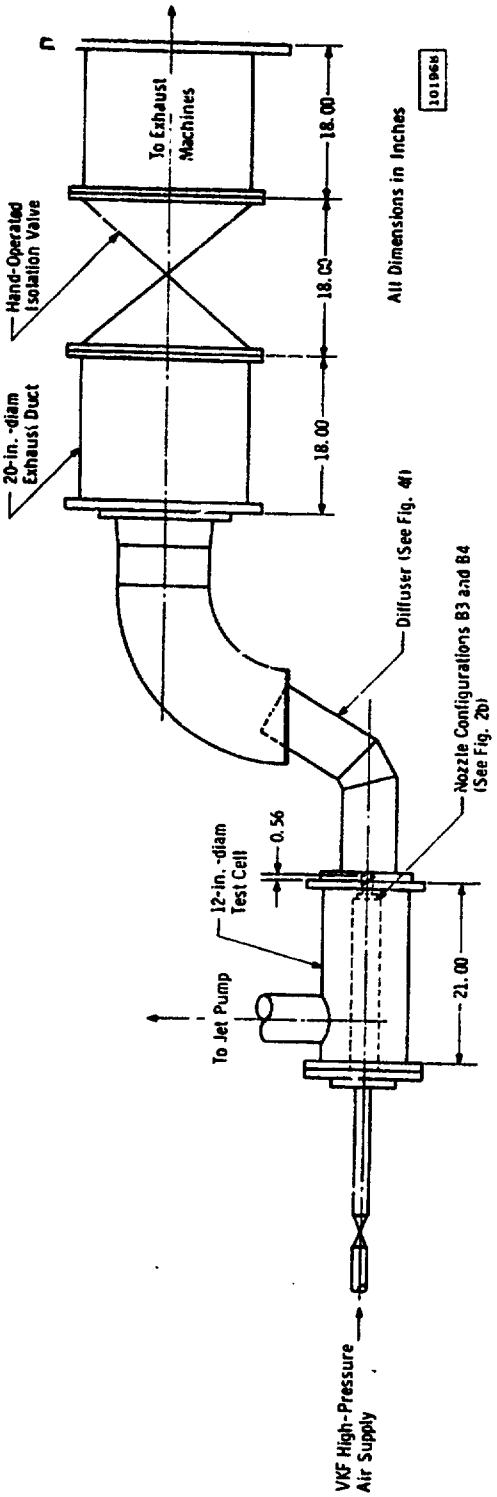

e. Diffuser Configuration 8 Installation

Fig. 1 Concluded

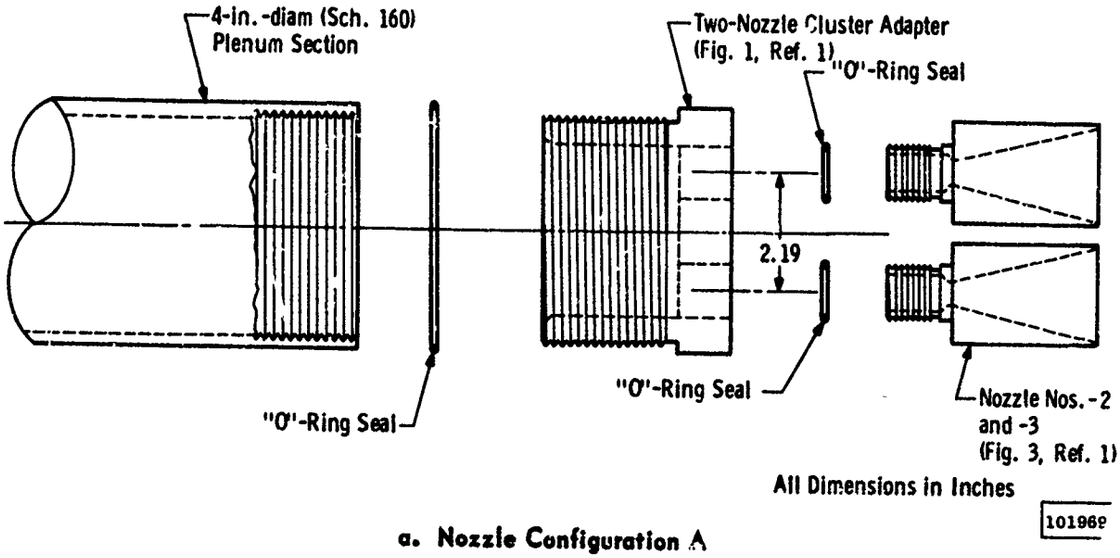

a. Nozzle Configuration A

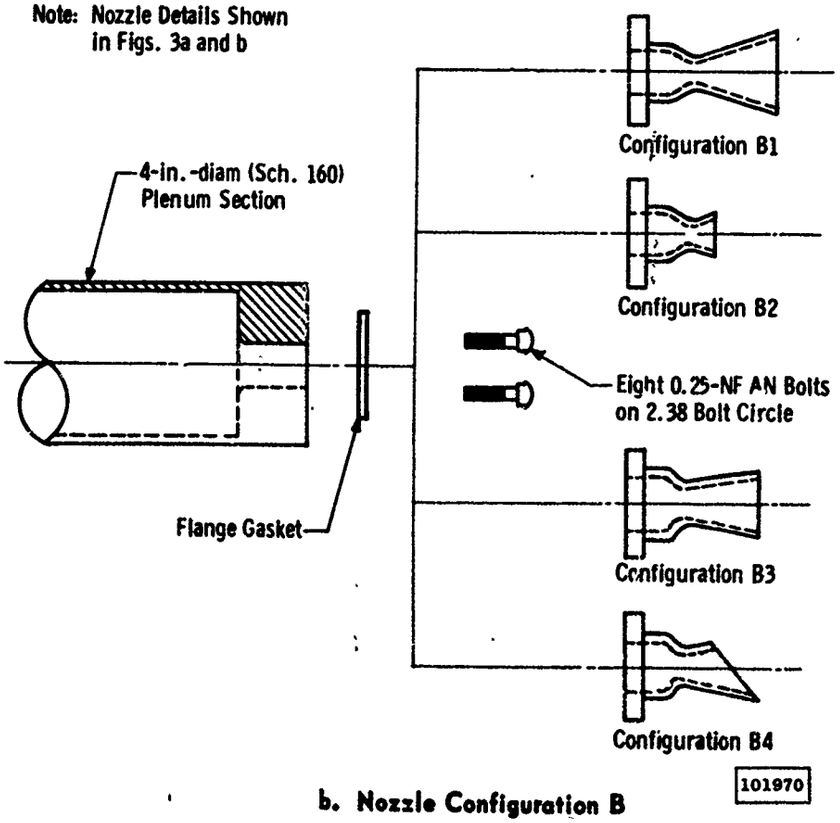

b. Nozzle Configuration B

Fig. 2 Simulated Rocket Nozzle Configurations

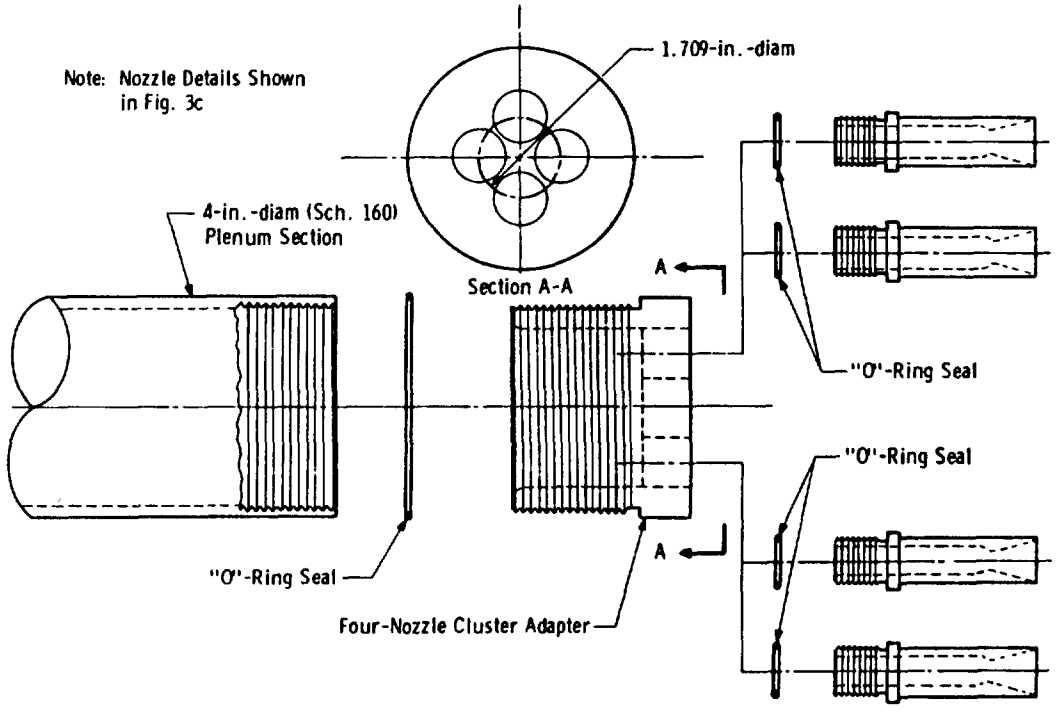

c. Nozzle Configuration C

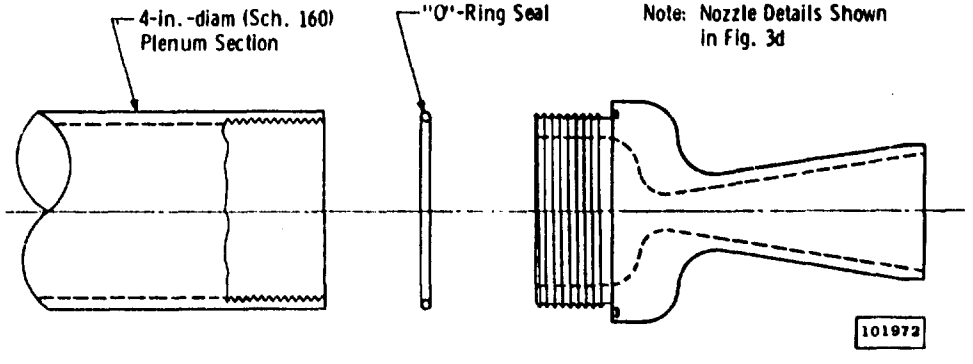

d. Nozzle Configuration D

Fig. 2 Concluded

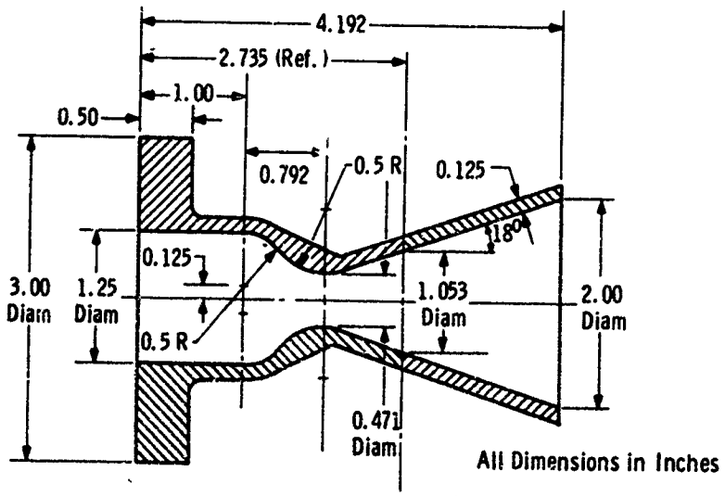

Nozzle No.	A_{ne}/A^*	Exit Diam, d_{ne}
1	16.00	2.00
2	5.00	1.053

a. Nozzle Numbers 1 and 2

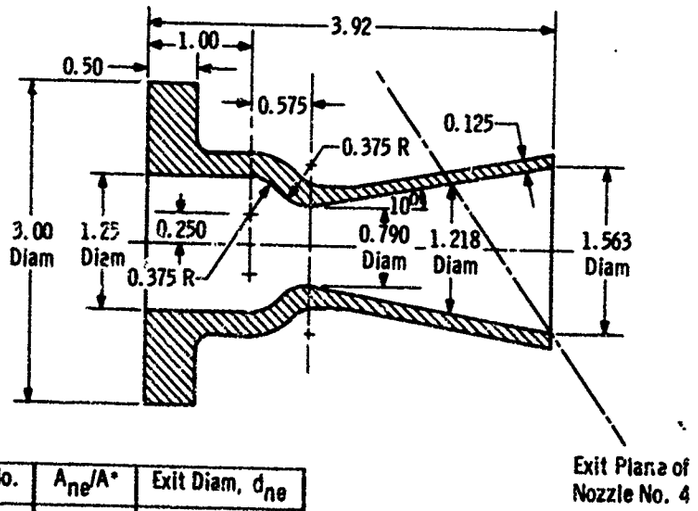

Nozzle No.	A_{ne}/A^*	Exit Diam, d_{ne}
3	3.914	1.563
4	3.147[1]	1.218

[1]Based on Average Nozzle Exit Area

b. Nozzle Numbers 3 and 4

Fig. 3 Simulated Rocket Nozzle Details

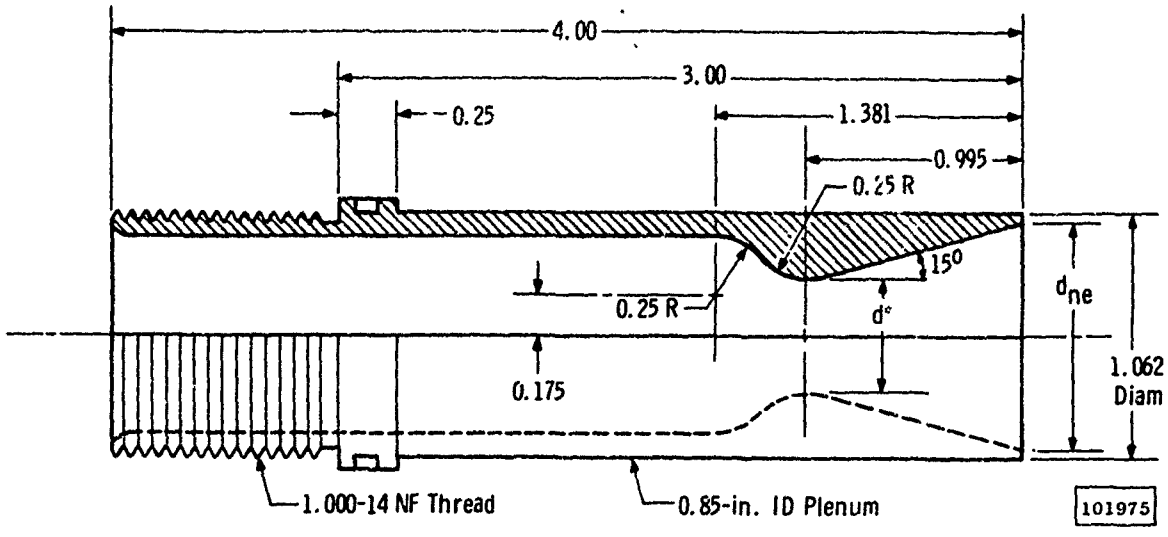

Nozzle No.	A_{ne}/A^*	Exit Diam, d_{ne}	Throat Diam, d^*
5	4.016	0.980	0.4890
6	4.207	1.005	0.4900
7	4.149	0.995	0.4885
8	4.107	0.990	0.4885

All Dimensions in Inches

c. Nozzle Numbers 5 through 8

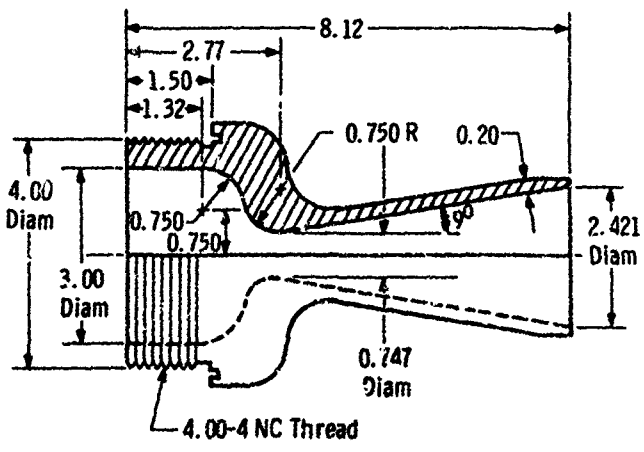

d. Nozzle Number 9

Fig. 3 Concluded

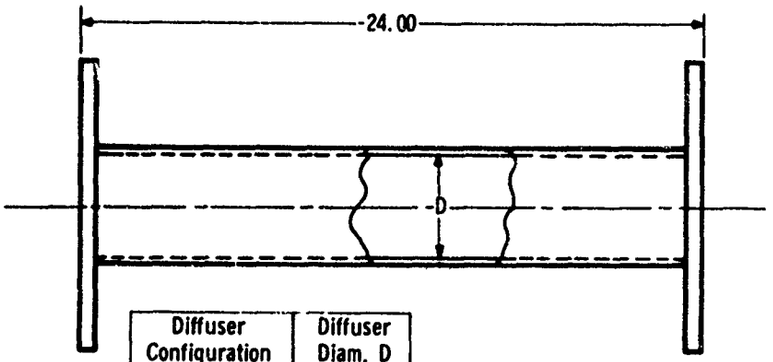

Diffuser Configuration	Diffuser Diam, D
1	4.026
3	6.141

All Dimensions in Inches

101977

a. Straight Cylindrical Diffuser Configurations 1 and 3

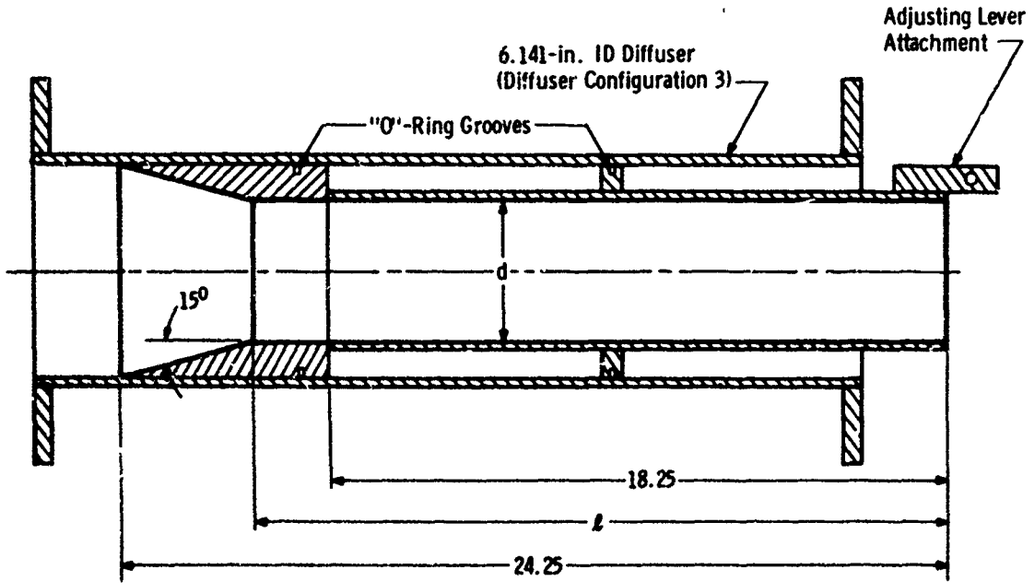

Diffuser Configuration	Second-Throat Diam, d	Second-Throat Length, ℓ
S3a	4.026	20.303
S3b	4.625	21.423
S3c	4.943	22.016

101978

b. Second-Throat Diffuser Configuration S3

Fig. 4 Diffuser Configurations and Details

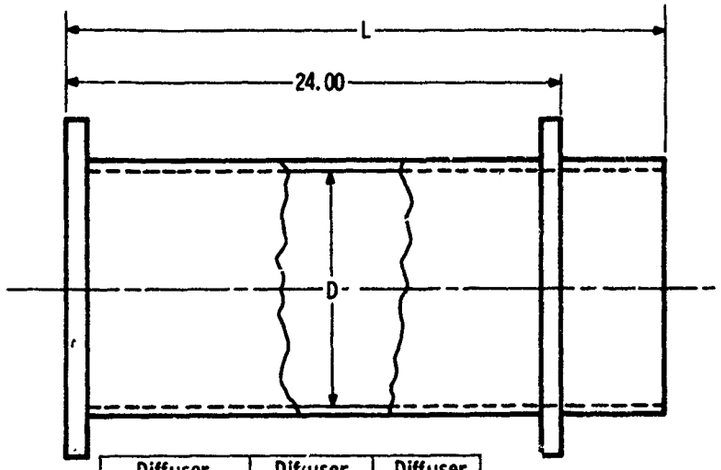

Diffuser Configuration	Diffuser Length, L	Diffuser Diam, D
2	25.500	4.680
4	31.438	8.092
5	46.500	10.020

101979

c. Straight Cylindrical Diffuser Configurations 2, 4, and 5

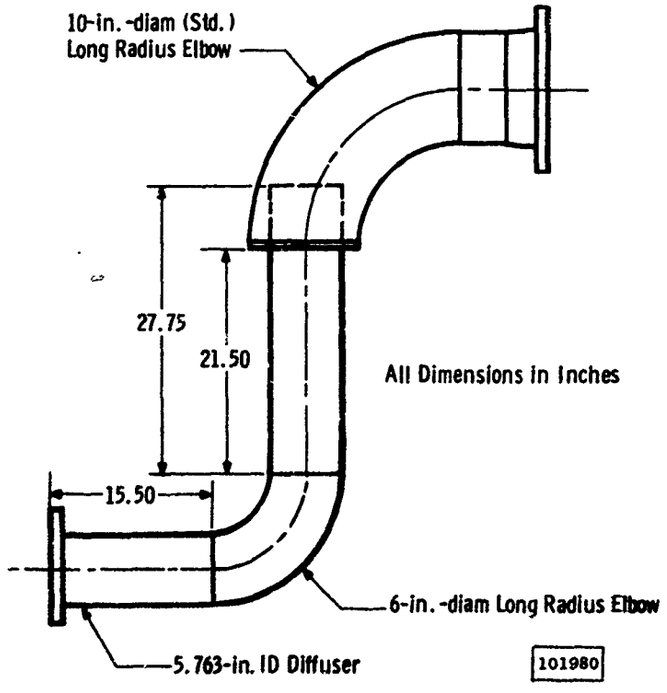

101980

d. Cylindrical Diffuser with 90-deg Long Radius Bend, Configuration 6

Fig. 4 Continued

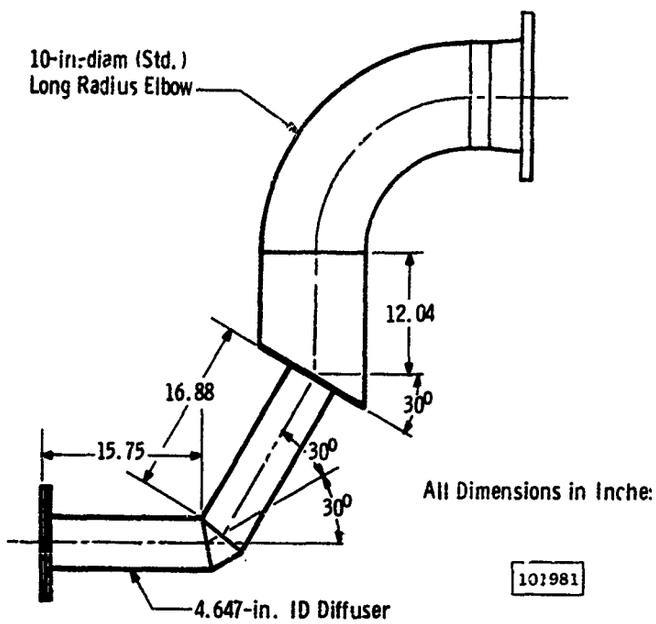

e. Cylindrical Diffuser with 60-deg Miter Bend, Configuration 7

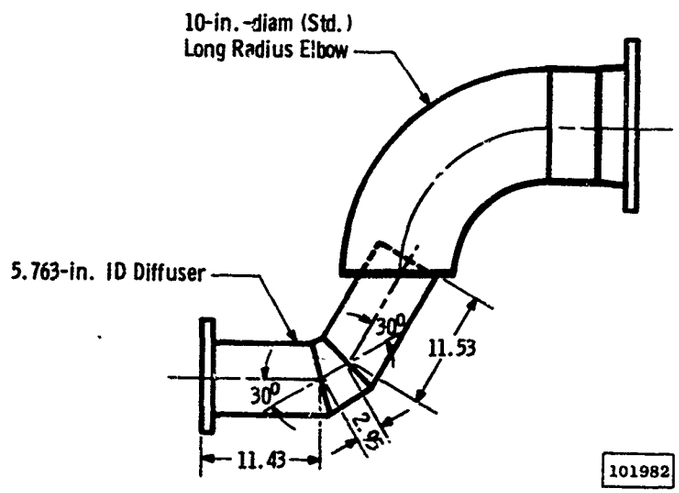

f. Cylindrical Diffuser with 60-deg Miter Bend, Configuration 8

Fig. 4 Concluded

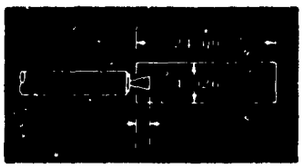

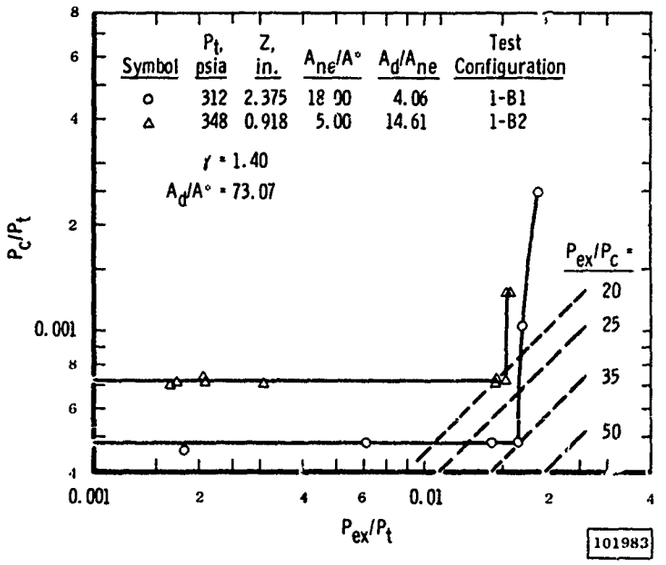

a. Configurations 1-B1 and 1-B2

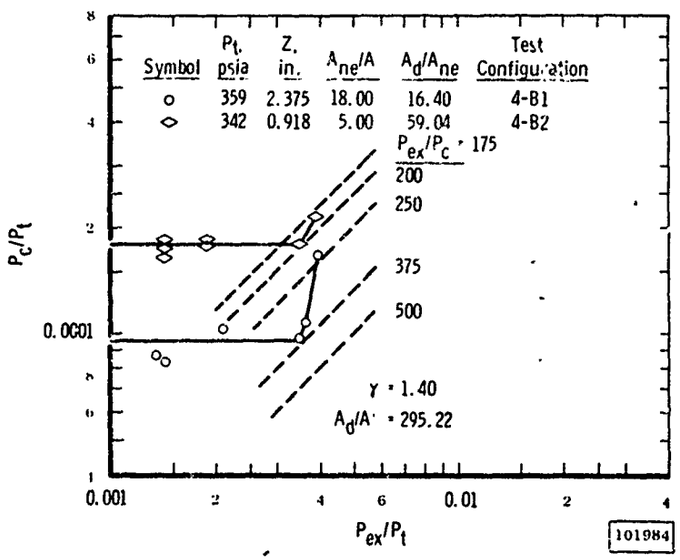

b. Configurations 4-B1 and 4-B2

Fig. 5 Ejector-Diffuser Performance for Different Average Nozzle Area Ratios

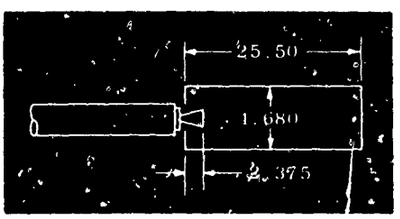

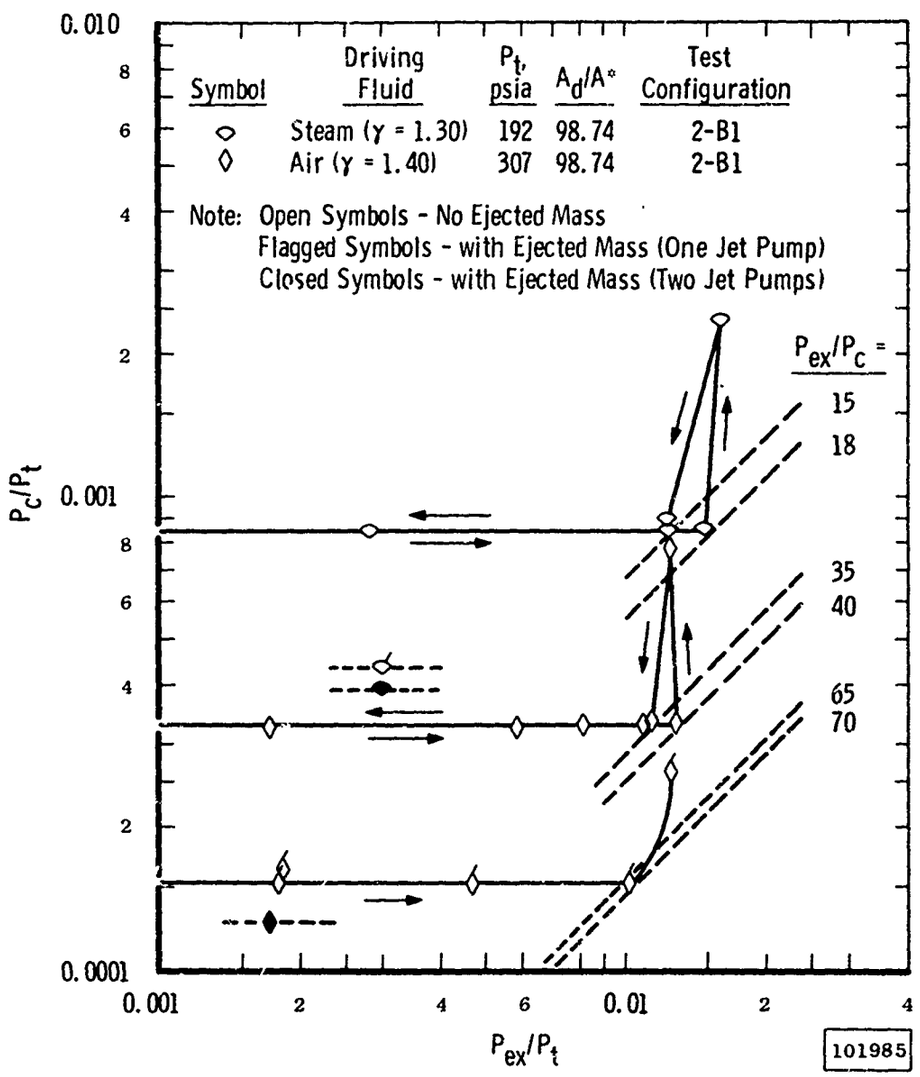

Fig. 6 Ejector-Diffuser Performance for Different Driving Fluids

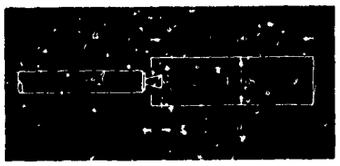

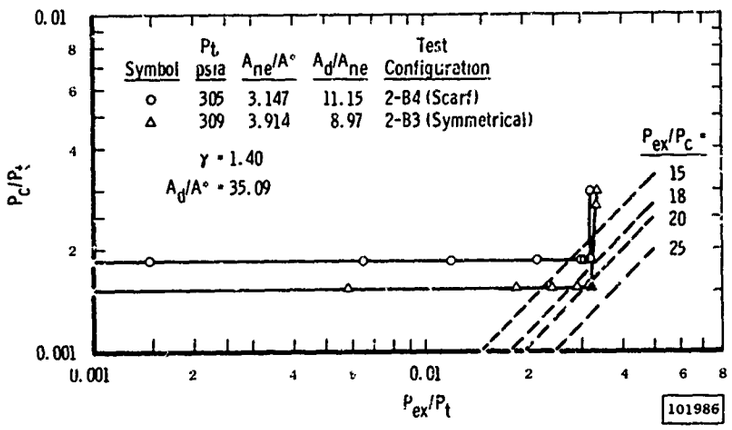

a. Configurations 2-B3 and 2-B4

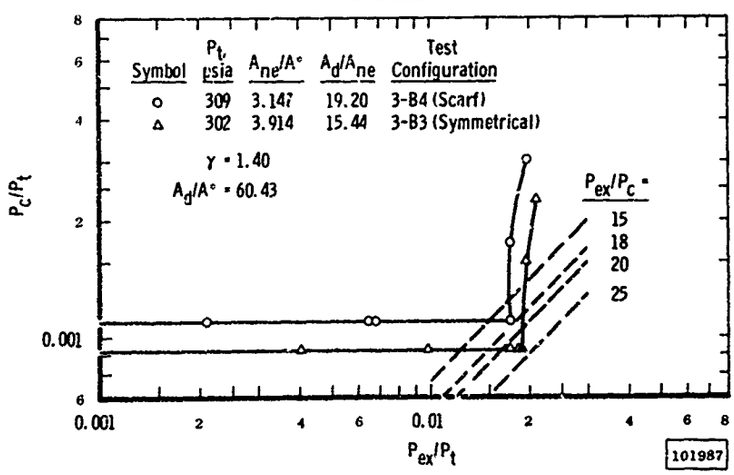

b. Configurations 3-B3 and 3-B4

Fig. 7 Comparison of Ejector-Diffuser Performance for Scarf and Symmetrical Nozzles

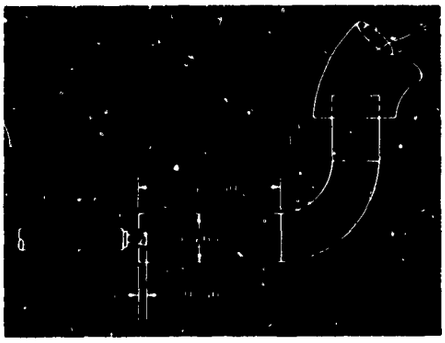

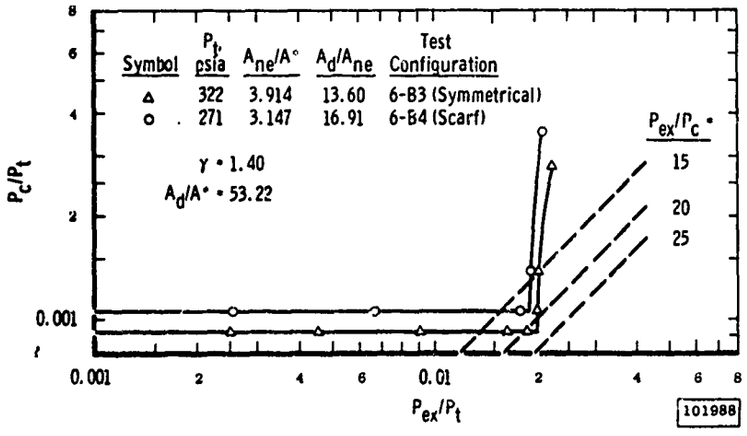

c. Configurations 6-B3 and 6-B4

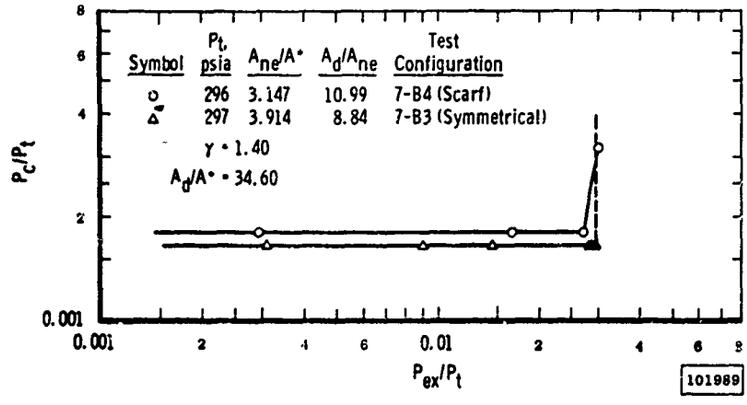

d. Configurations 7-B3 and 7-B4

Fig. 7 Continued

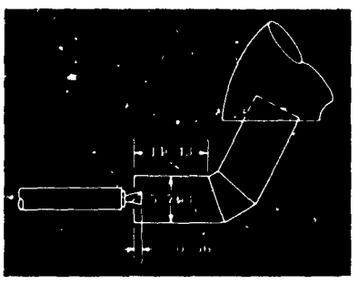

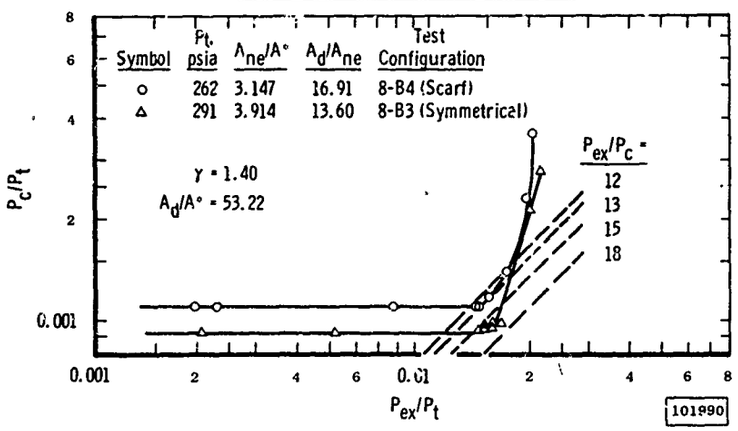

e. Configurations 8-B3 and 8-B4

Fig. 7 Concluded

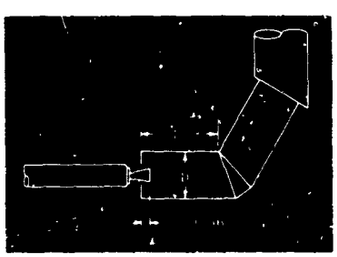

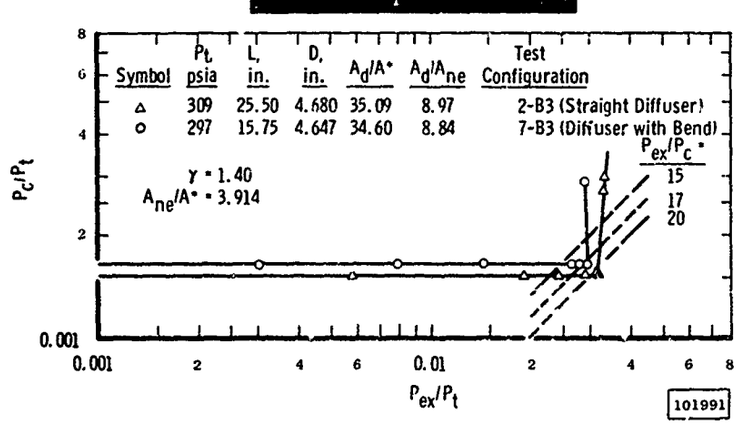

Fig. 8 Comparison of Ejector-Diffuser Performance for Straight Diffusers and Diffusers with Bends

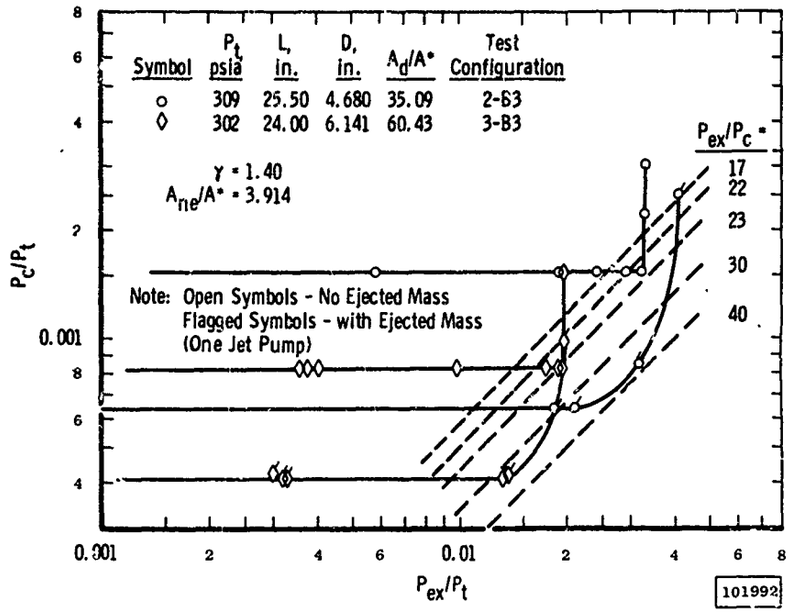

a. Configurations 2-B3 and 3-B3 (Symmetrical Nozzle)

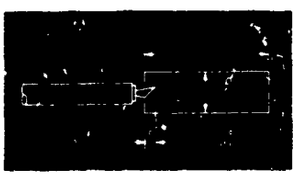

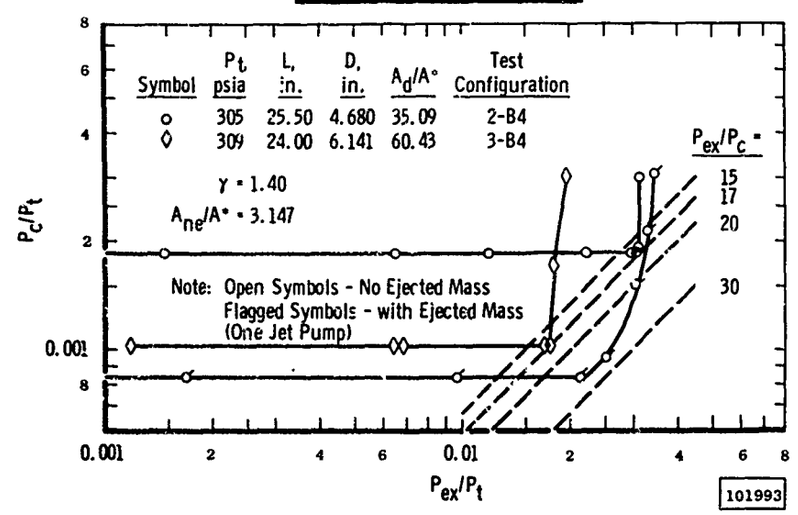

b. Configurations 2-B4 and 3-B4 (Scarf Nozzle)

Fig. 9 Ejector-Diffuser Performance with and without Ejected Mass from the Test Cell

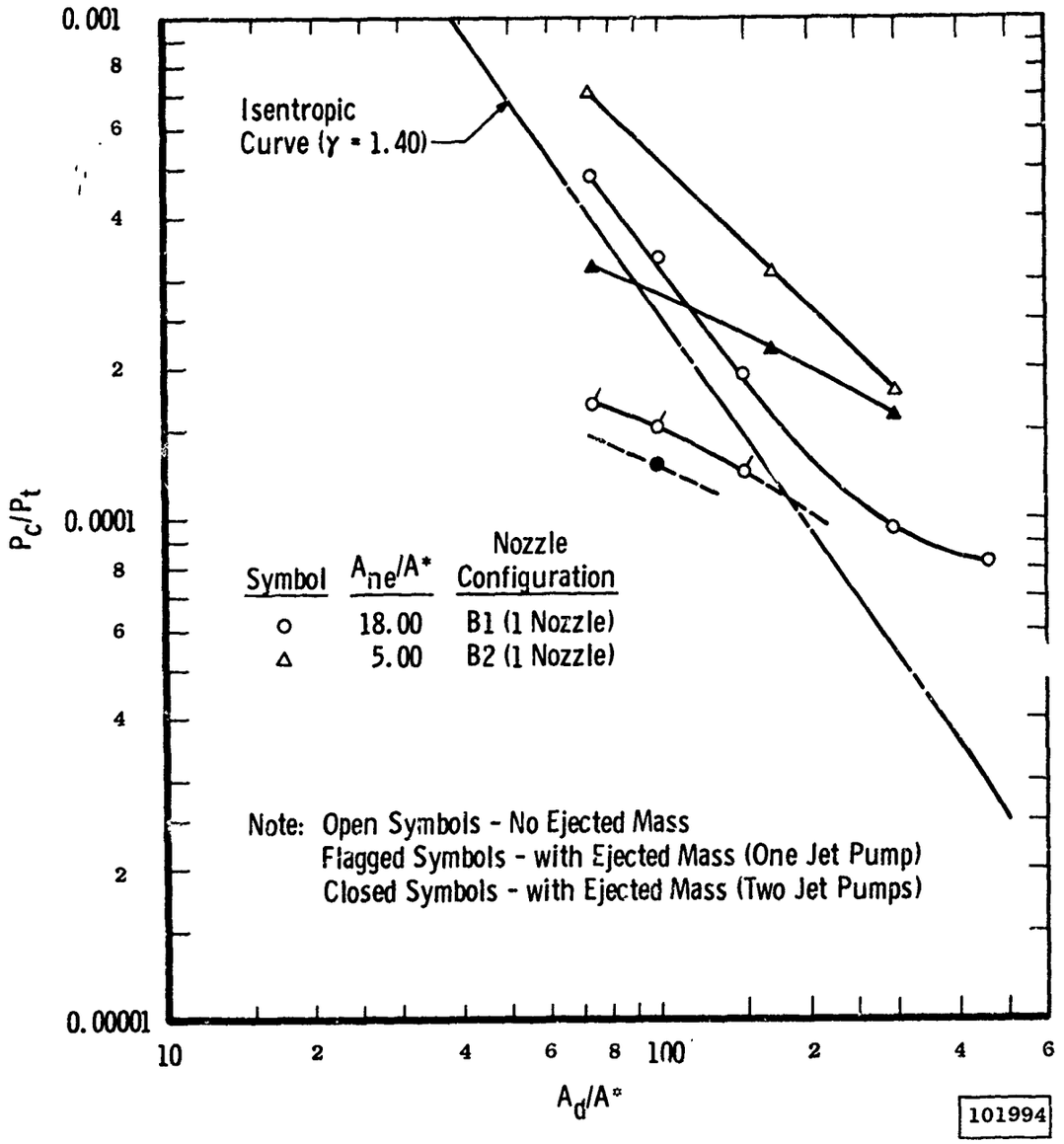

a. Diffuser Configurations 1 through 6, Nozzle Configurations B1 and B2

Fig. 10 Variation of P_c/P_t with A_d/A^* Compared with One-Dimensional Isentropic P_c/P_t for Different Average A_{ne}/A^*

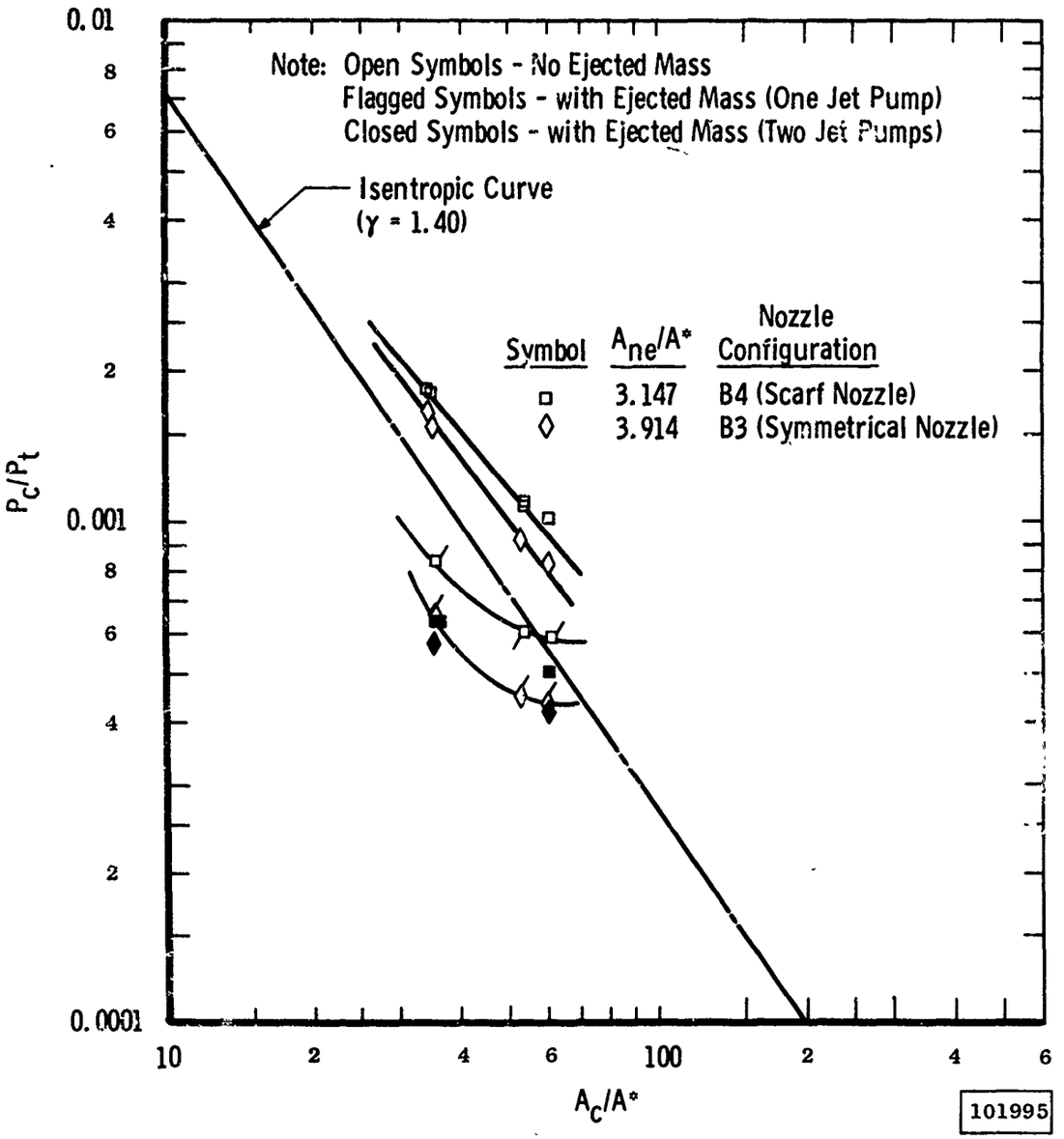

b. Diffuser Configurations 2, 3, 6, 7, and 8, Nozzle Configurations B3 and B4

Fig. 10 Continued

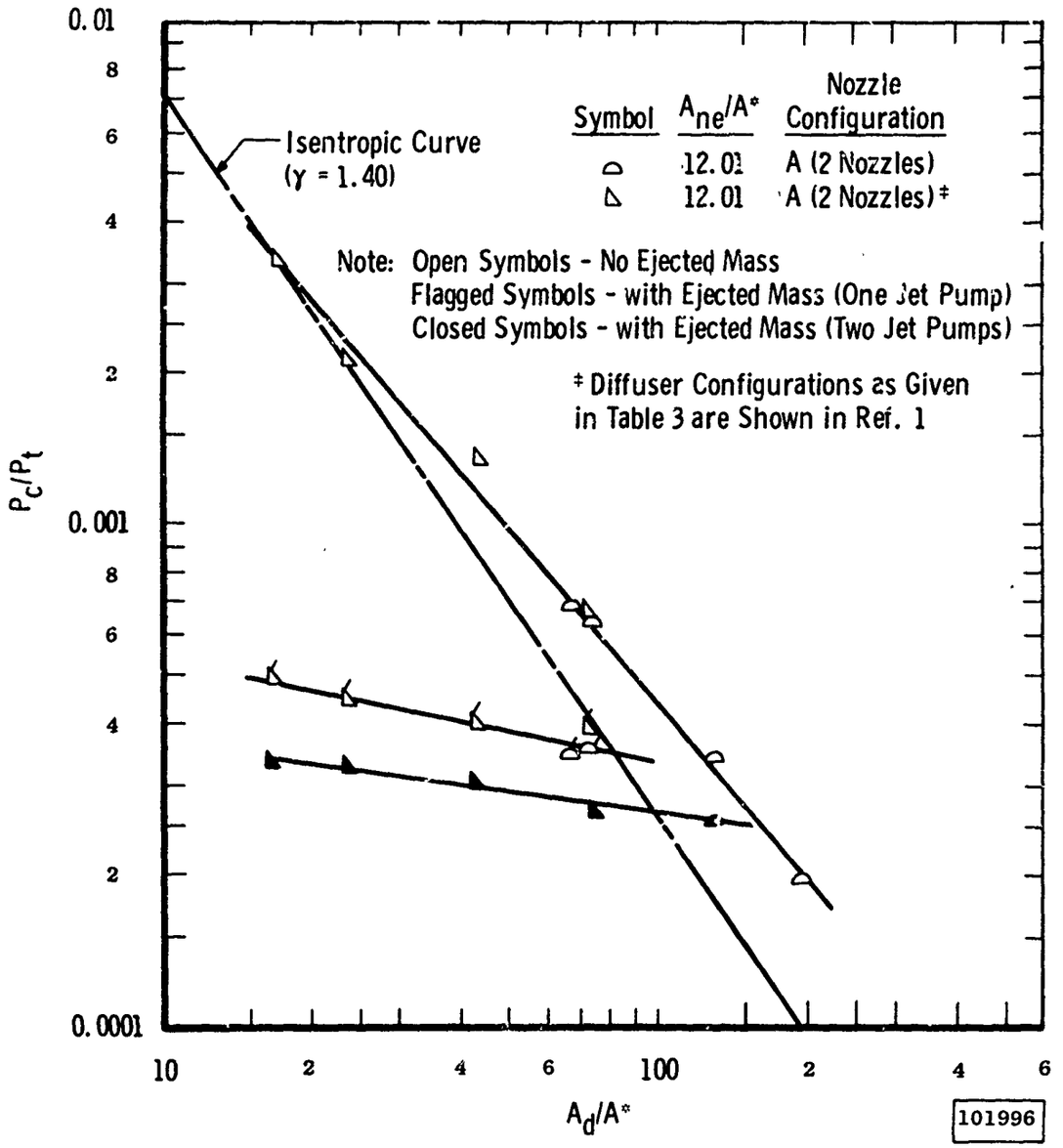

c. Diffuser Configurations 3 through 6, Nozzle Configuration A

Fig. 10 Continued

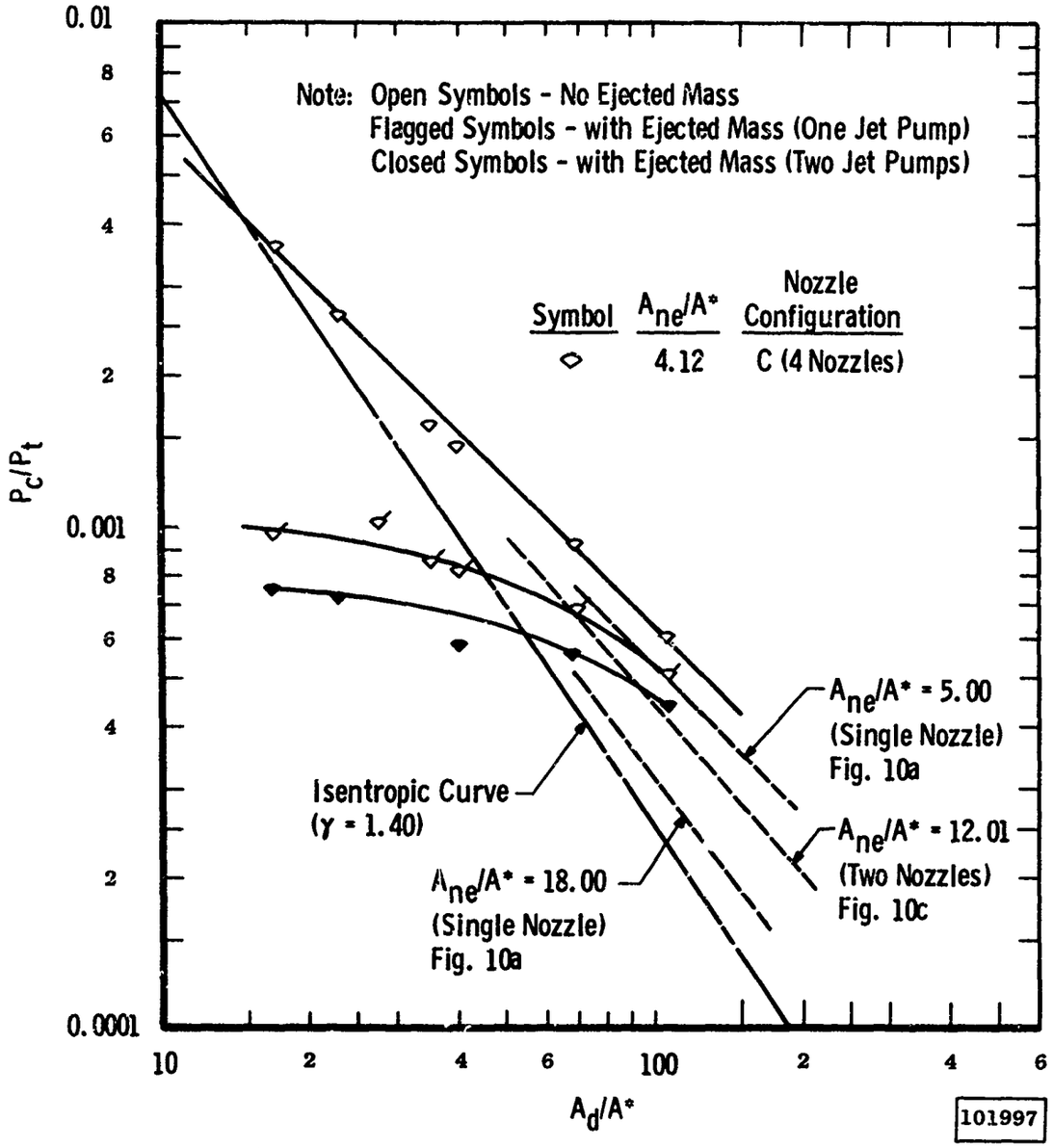

d. Diffuser Configurations 1 through 6, Nozzle Configuration C

Fig. 10 Concluded

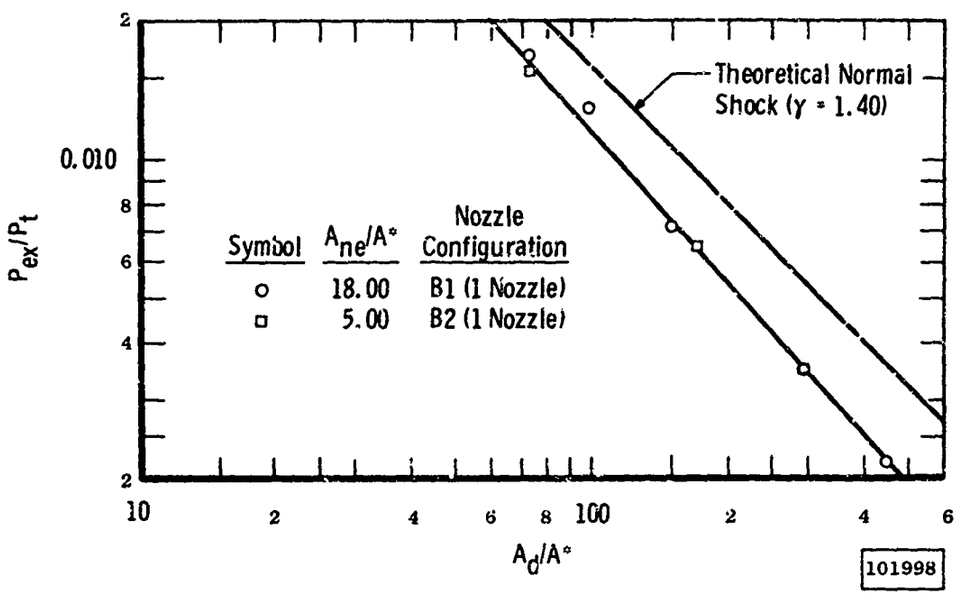

a. Diffuser Configurations 1 through 6, Nozzle Configurations B1 and B2

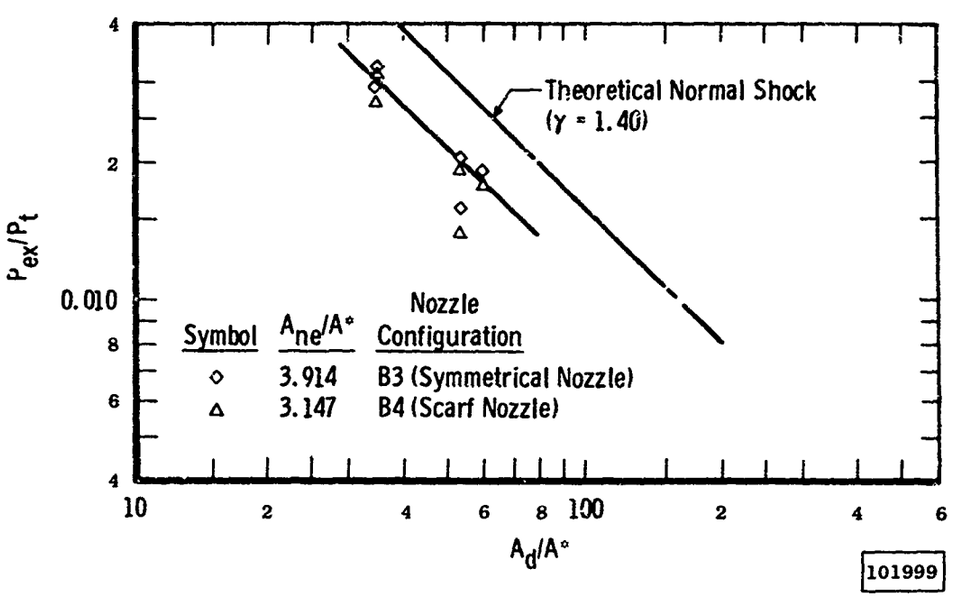

b. Diffuser Configurations 2, 3, 6, 7, and 8, Nozzle Configurations B3 and B4

Fig. 11 Ejector-Diffuser Average Starting Pressure Ratio Required for Different Nozzle Configurations

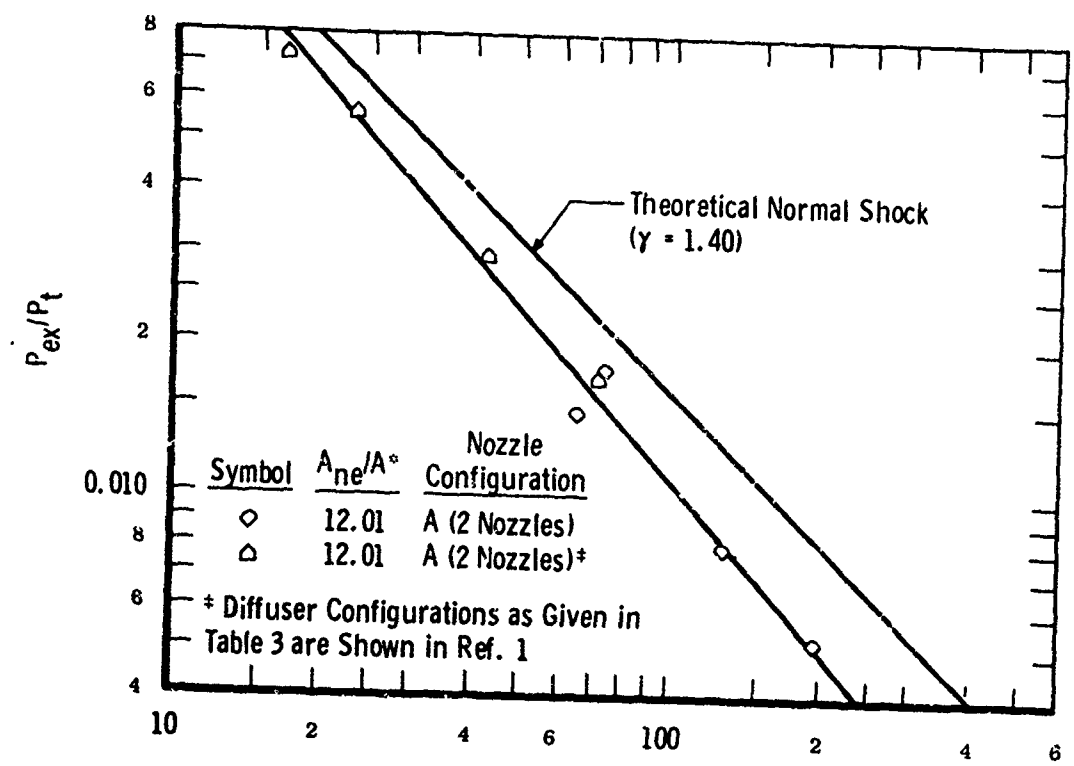

c. Diffuser Configurations 3 through 6, Nozzle Configuration A

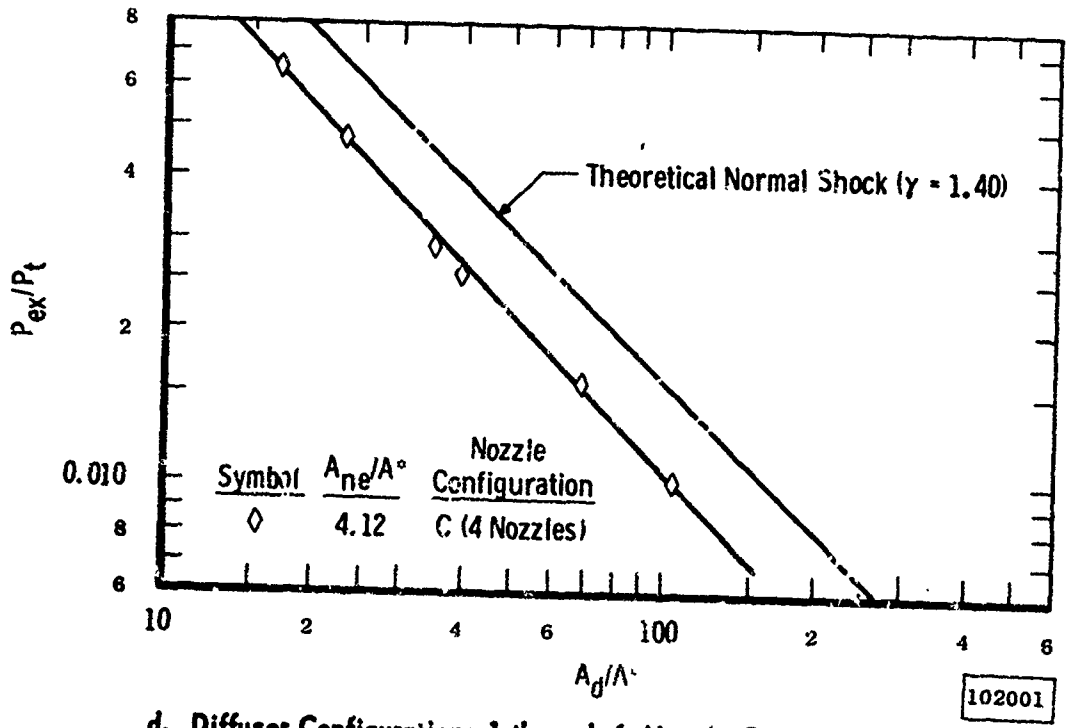

d. Diffuser Configurations 1 through 6, Nozzle Configuration C

Fig. 11 Concluded

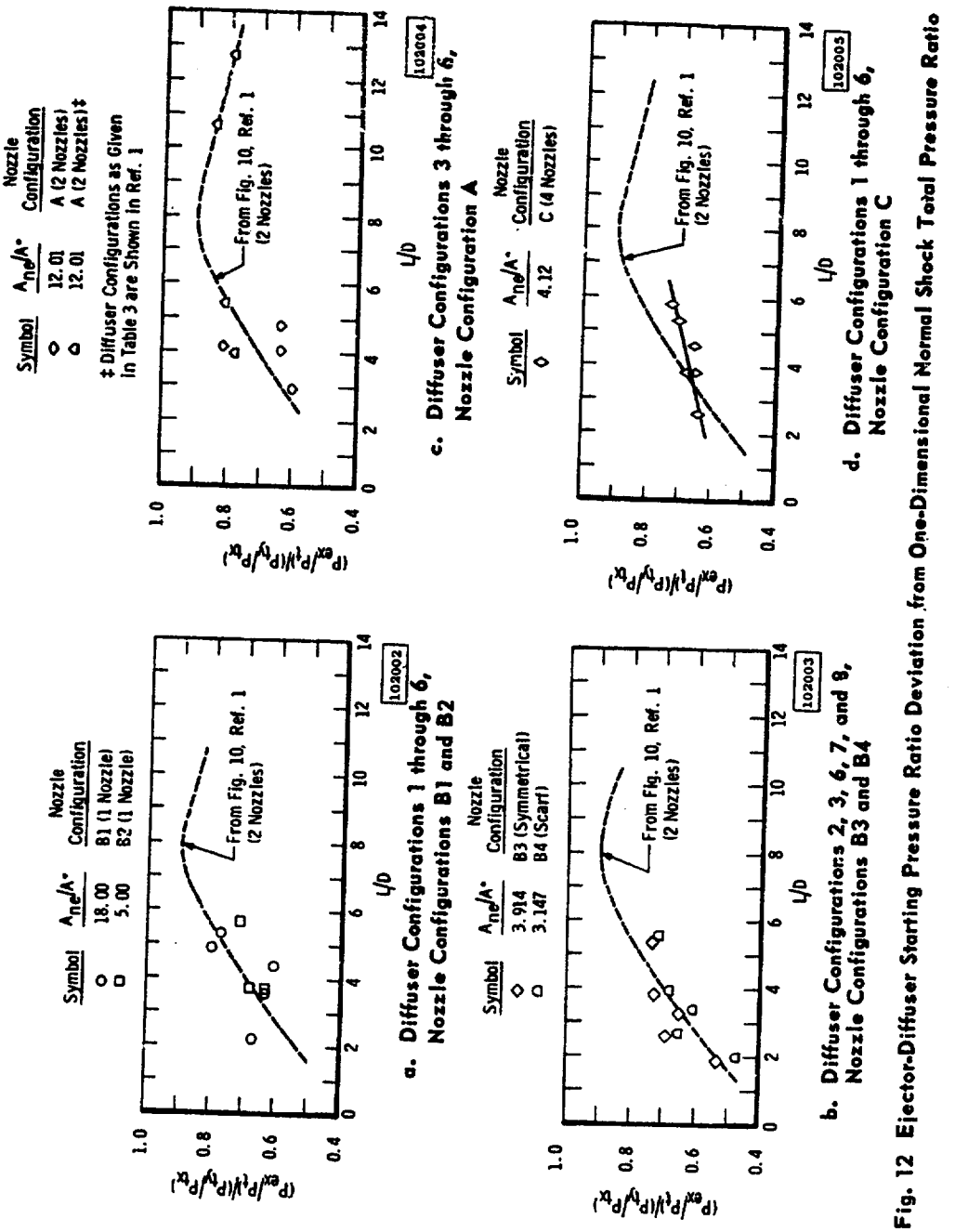

Fig. 12 Ejector-Diffuser Starting Pressure Ratio Deviation from One-Dimensional Normal Shock Total Pressure Ratio

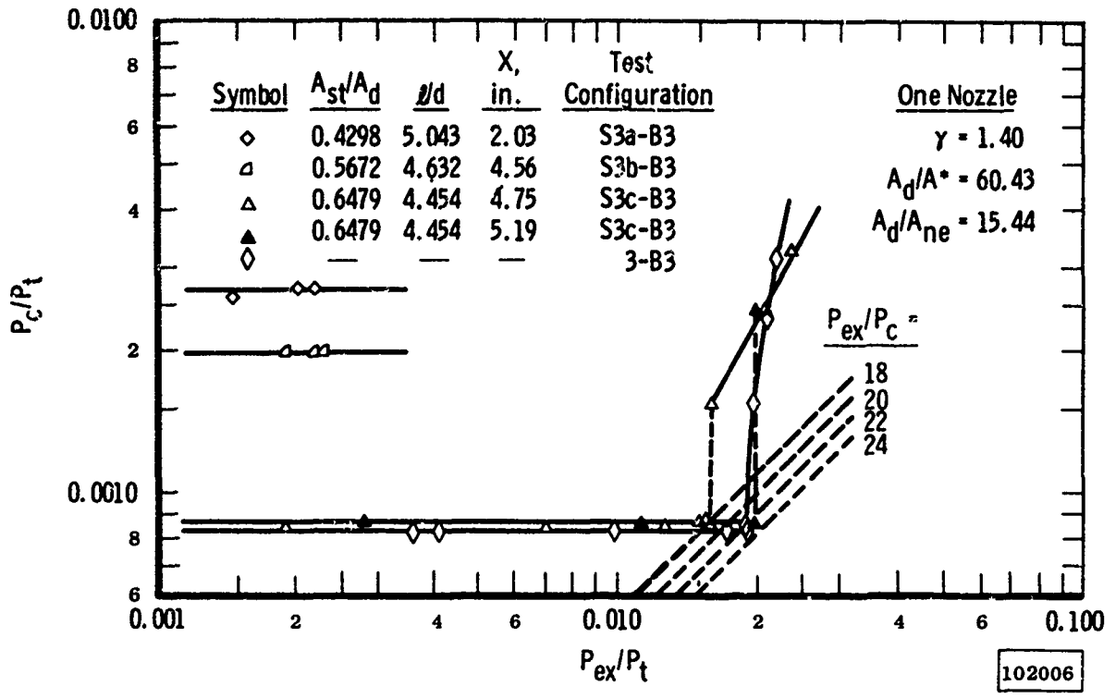

a. Configurations S3-B3 and 3-B3

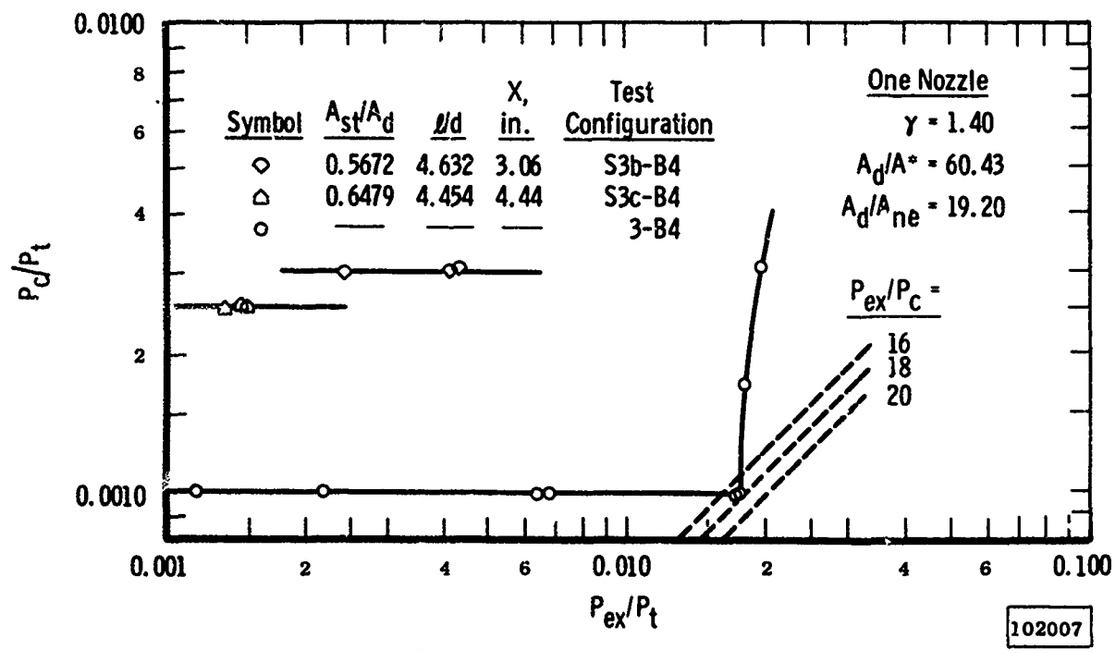

b. Configurations S3-B4 and 3-B4

Fig. 13 Effect of Second-Throat Contraction and Location on Ejector-Diffuser Performance

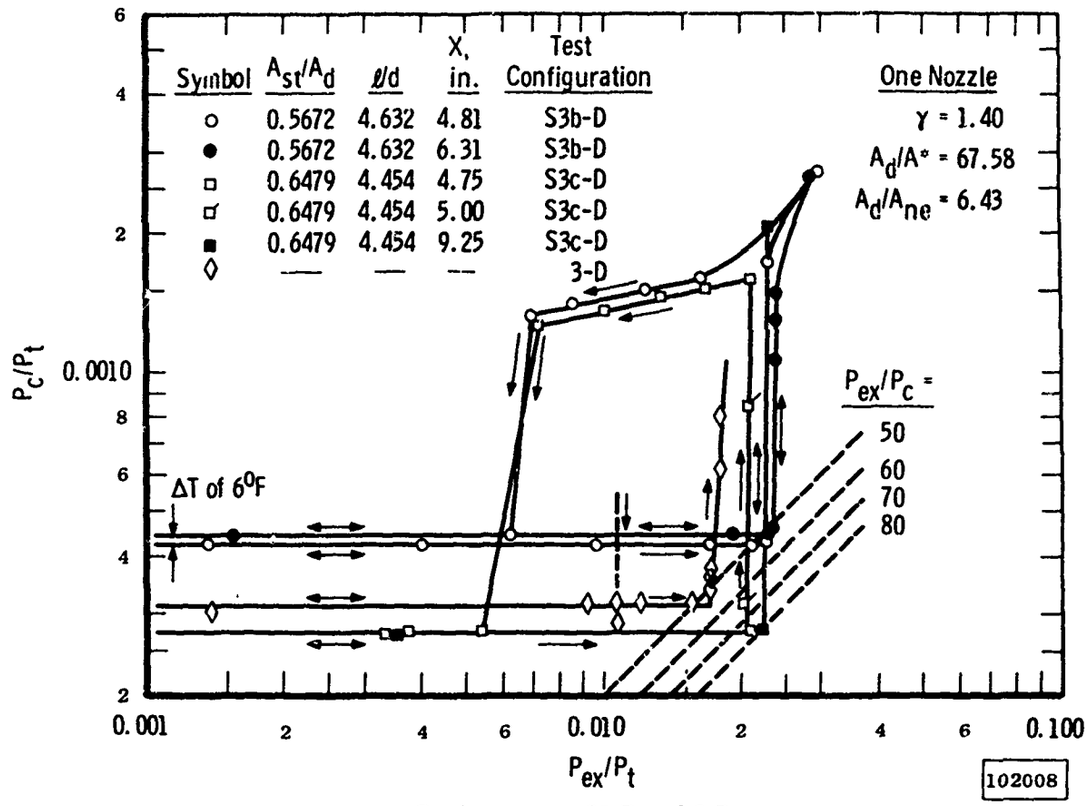

c. Configurations S3-D and 3-D

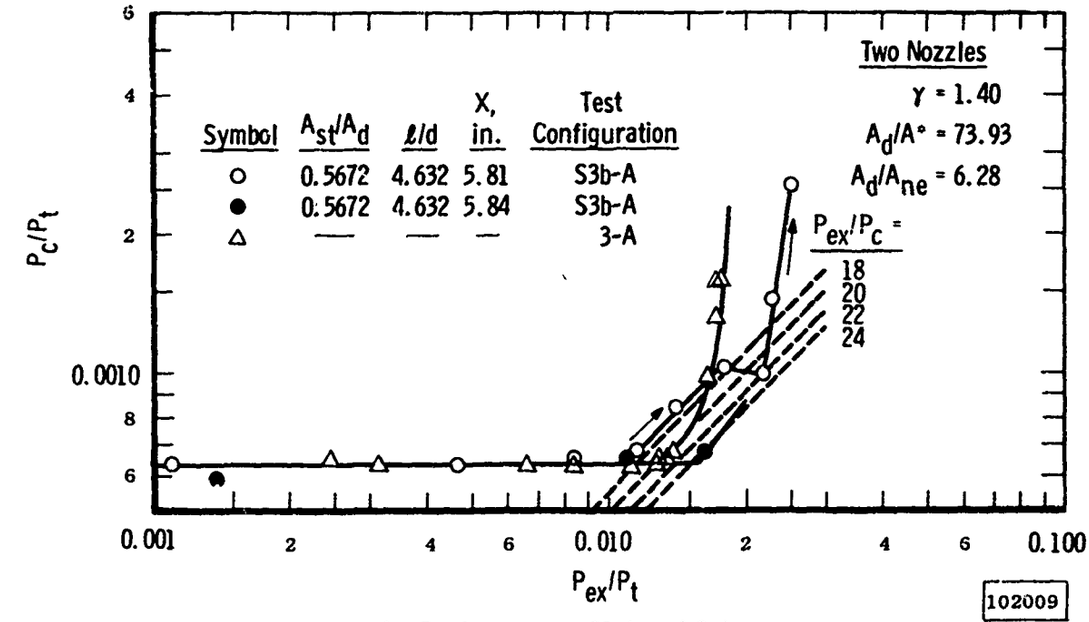

d. Configurations S3-A and 3-A

Fig. 13 Continued

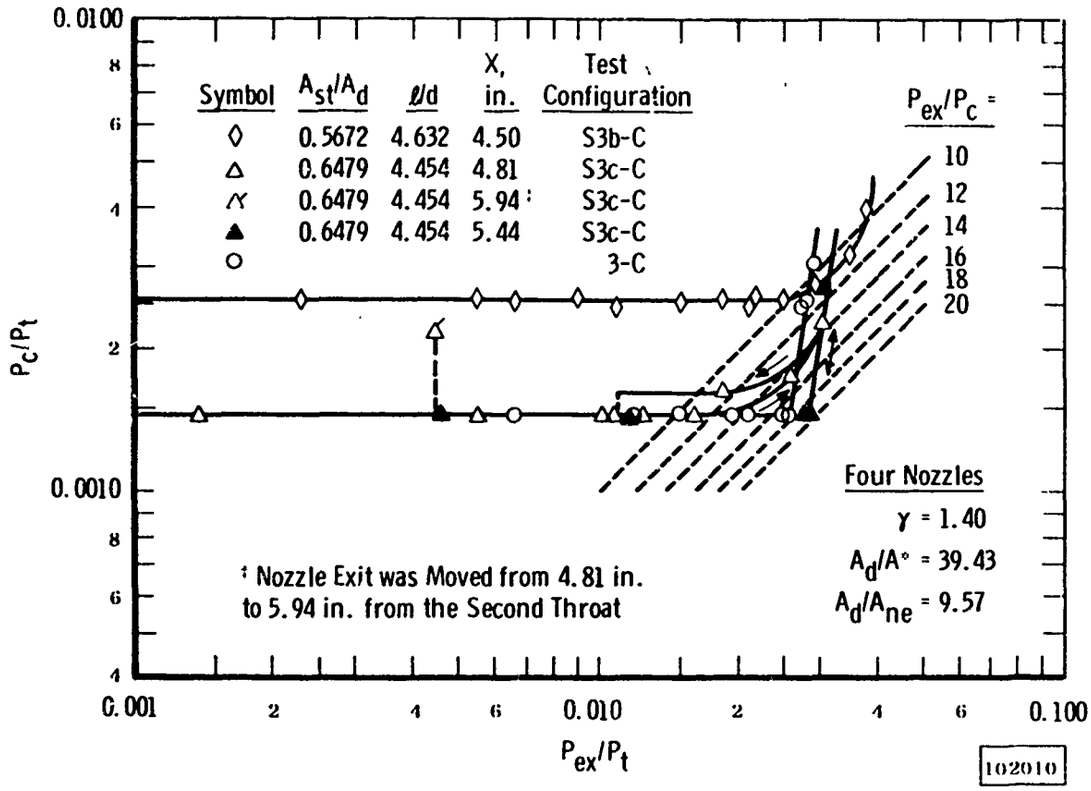

e. Configurations S3-C and 3-C

Fig. 13 Concluded